

# L-dwarf variability: *I*-band observations

Christopher R. Gelino, Mark S. Marley<sup>1</sup>, Jon A. Holtzman

*Department of Astronomy, New Mexico State University, Las Cruces, NM, 88003*

crom@nmsu.edu, mmarley@mail.arc.nasa.gov, holtz@nmsu.edu

Andrew S. Ackerman

*NASA Ames Research Center, Moffett Field, CA, 94035*

ack@sky.arc.nasa.gov

and

Katharina Lodders

*Planetary Chemistry Laboratory, Department of Earth and Planetary Sciences, Washington University, St. Louis, MO, 63130*

lodders@levee.wustl.edu

## ABSTRACT

We report on the results of an *I*-band photometric variability survey of eighteen L dwarfs. We find that seven exhibit statistically significant variations above the 95.4% confidence level with root-mean-square scatter (including photometric errors) between 0.010 and 0.083 mag. Another five targets have variability probabilities  $\approx 80\%$ , suggesting that these are likely variable objects. Three of the variable objects display significant peaks in a CLEAN periodogram that are several times higher than the noise. The period for 2MASS 0345+25 is clearly not intrinsic to the object and can be dismissed. The periods found for 2MASS 0746+20AB and 2MASS 1300+19 are unique but longer than those periods likely from rotation velocity measurements and they do not represent periodic behavior in the light curve that persists through the entire data set. These observations suggest that we are not observing the rotation modulation of a long-lived albedo feature. Instead, rapid evolution of atmospheric features is likely causing the

---

<sup>1</sup>NASA Ames Research Center, Moffett Field, CA, 94035

non-periodic variability. The remaining variable objects show no prominent features in their light curves, suggesting even more rapid evolution of atmospheric features. We argue against the existence of magnetic spots in these atmospheres and favor the idea that non-uniform condensate coverage is responsible for these variations. The magnetic Reynolds number in the atmosphere of L dwarfs is too small to support the formation of magnetic spots. In contrast, silicate and iron clouds are expected to form in the photospheres of L dwarfs. Inhomogeneities in such cloud decks and the evolution of the inhomogeneities can plausibly produce the observed photometric variations.

*Subject headings:* stars: atmospheres — stars: low mass, brown dwarfs

## 1. Introduction

Large numbers of L dwarfs (Kirkpatrick et al. 1999; Martín et al. 1999; Basri et al. 2000; Kirkpatrick et al. 2000) are being discovered by surveys such as the 2 Micron All Sky Survey (2MASS) and the Sloan Digital Sky Survey (SDSS). Despite their growing number, less than 10% of known L dwarfs have been observed to determine whether or not they are photometrically variable (Tinney & Tolley 1999; Bailer-Jones & Mundt 1999, 2001a; Clarke, Tinney, & Covey 2002). Photometric monitoring of L dwarfs, and brown dwarfs in general, not only explores why some objects are variable while others are not, but it can also help constrain rotation periods or timescales for the evolution of surface features. Multicolor photometric and spectroscopic monitoring could even be used to identify the nature of those features.

Tinney & Tolley (1999) presented the first attempt to detect clouds in brown dwarf atmospheres. They observed the M9 brown dwarf LP944–20 and the L5 brown dwarf DENIS 1228–15 through two narrow-band filters chosen to detect changes in TiO absorption. The changes in the TiO band strength were presumed to indicate changes in the opacity, which occurs when TiO is depleted through condensation. They found that LP944–20 was variable, but DENIS 1228–15 was not. The authors speculated that the passage of clouds over the disk of LP944–20 produced small changes in the brightness temperature in their narrow-band filters and caused small variations ( $\sim 0.04$  magnitude). However, the lack of variability in their L dwarf does not exclude the possibility of clouds in that object since the variations observed in LP944–20 had smaller amplitudes than the errors for DENIS 1228–15.

Bailer-Jones & Mundt (1999) conducted a variability search in the broad-band  $I$  filter and found evidence of variability in the L1.5 dwarf 2MASS 1145+23. The object displayed

$\sim 0.04$  magnitude variations that repeated with a period of 7.1 hours. In an expanded study of 21 L and M dwarfs Bailer-Jones & Mundt (2001a,b) found that over half of their sample exhibited statistically significant variations with root-mean-square (RMS) scatter between 0.010 and 0.055 magnitude and time scales of 0.4 to 100 hours. They were unable to find periodic light curves for many of the variables. 2MASS 1145+23, however, exhibited variability with a period of 11.2 hours. They suggested that evolving surface features, possibly dust clouds or magnetic spots, were responsible for the change in period. A similar varying period has also been observed in the M9.5 dwarf star BRI0021 by Martín, Zapatero Osorio, & Lehto (2001).

Photometric variability has recently been reported for the L2 dwarf Kelu-1 (Clarke et al. 2002). Like Tinney & Tolley (1999), these authors use a special filter positioned at a region sensitive to changes in TiO and CrH absorption. Kelu-1 displayed small ( $\sim 1.1\%$ ) peak-to-peak variations that phased well to a period of 1.8 hours.

Either magnetic spots or clouds could plausibly be associated with the observed variability. Magnetic fields have been measured for several M dwarfs and estimates of their strength are a few kG (Saar 1994; Johns-Krull & Valenti 1996), with surface filling factors generally  $> 50\%$ . Periodic photometric variations have been observed in only a few M dwarfs, suggesting that either the surfaces of these objects are completely covered with spots or that the spots are few in number and uniformly distributed (Hawley, Reid, & Gizis 2000). In addition, Bondar (1995) reports that no good data exist to support the scenario of cyclic, organized spots in M dwarfs cooler than M0.

For the L dwarfs, clouds are a reasonable potential source of variability. Iron, enstatite, and forsterite are the most abundant species expected to condense at the atmospheric temperatures and pressures characteristic of the L dwarfs (Lodders 1999; Burrows & Sharp 1999). Once condensed, the species likely settle into discrete, optically thick, cloud decks, with optically thicker clouds arising in progressively later L dwarfs (Marley 2000; Ackerman & Marley 2001). Since the atmospheric circulation pattern of most L dwarfs is likely similar to that of Jupiter (Schubert & Zhang 2000), it is not unreasonable to expect that many L dwarfs also have a banded appearance. Any large inhomogeneities (thicker clouds or clearings in the cloud deck) could then produce a photometric signal. Gelino & Marley (2000) show that if Jupiter were to be observed in thermal emission as an unresolved point source, the Great Red Spot would provide a photometrically detectable signal. If L dwarfs have similar cloud features to Jupiter, then it is plausible that they may also exhibit photometric variations.

We are conducting a photometric monitoring program of L dwarfs in the  $I_C$  band. In this study we present the light curves for several L dwarfs showing statistically significant

variability. We discuss which of these display significant periodicity and why the others do not. We provide theoretical calculations that reject the magnetic spot hypothesis for the origin of the variation and argue in favor of clouds.

## 2. Observations

### 2.1. Target Selection

Our target list was derived from a compilation of all published spectroscopically determined L dwarfs. We searched the list for all L dwarfs above  $\delta = -10^\circ$  and brighter than  $I \approx 18$ . For the objects whose  $I$  magnitudes had not been measured we estimated their brightness in that filter based upon the objects' spectral types and the  $I - J$  colors from Kirkpatrick et al. (1999). Better estimates of these  $I$  magnitude were made after observations using instrumental magnitudes and  $I - J$  colors.

At the start of this project there were 24 objects that fit these criteria. Table 1 lists the 18 L dwarfs in our sample that were observed. Except for an L4, we have at least one object for each decimal subclass between L0 and L4.5, inclusive. All are discoveries from the 2MASS survey (Gizis et al. 2000; Kirkpatrick et al. 1999, 2000) and are field objects. Their  $I$ -band magnitudes range from 15.11 mag (measured) to  $\sim 18.1$  mag (estimated). Finally, exactly half of the sample has measurable  $H\alpha$  emission.

2MASS 0746+20AB and 2MASS 1146+22AB are close visual binaries as seen with Keck and the Hubble Space Telescope (Koerner et al. 1999; Reid et al. 2001) and are unresolved in our observations. Reid et al. (1999) state that Keck echelle spectroscopy indicate 2MASS 0345+25 is a spectroscopic binary. However, additional spectra of 2MASS 0345+25 can neither confirm nor reject the possibility of a binary system (Reid 2001, private communication). Only two other targets were observed for binarity (2MASS 0036+18 and 2MASS 1338+41; Reid et al. 2001), but none was found. However, nearly 25% of all L dwarfs observed in binary studies are shown to be binaries. Therefore, the probability that other binaries exist in our sample is quite high.

### 2.2. Data Acquisition

We used the New Mexico State University 1m telescope at Apache Point Observatory for our observations. The telescope was equipped with an Apogee 512 $\times$ 512 pixel, thermoelectrically cooled CCD with a pixel scale of 0.8 arcsec/pixel and was operated robotically.

For each cycle the telescope was focused on a bright star and the script chose one to three targets that had airmasses between 1.03 and 1.9. After slewing to a target, the telescope pointing was refined by slewing to a nearby bright standard star and centering the star in the CCD. The telescope reslewed to the target and found a guide star from the USNO-SA2.0 catalog (Monet et al. 1998). On most nights three consecutive 5 minute exposures were taken in the Cousins *I* band for each target; no other filters or exposure times were used. This cycle was repeated as many times as possible throughout the night. Each target was usually observed every 1-2 hours in a given night, depending on the target’s hour angle and priority.

Observations for this program started on 2000 October 30 and ended on 2001 June 20. During this period the telescope was used as much as possible for this program. Observations were taken at all moon phases and under a variety of seeing conditions. Over 3700 science images (not including positional calibration frames and focus runs) were obtained, resulting in over 300 hours of on-sky time for science observations. As with any observing program, time was occasionally lost due to inclement weather and engineering problems. The longest off-sky period was approximately 1 month from mid-December to mid-January.

### 2.3. Data Reduction

The images were reduced using procedures in the XVISTA astronomical image reduction and analysis package. All images were first dark subtracted and then flat fielded. Finally, a correction was applied to reduce the effect of night sky emission line fringing in the frames. These steps are discussed in more detail below.

#### 2.3.1. Dark Subtraction

Dark current is an additive noise that depends strongly on the operating temperature of the CCD and the exposure time. The amount of charge accumulated increases with the exposure time; the rate of charge production increases with increasing temperature. We limited our thermo-electrically cooled CCD to be set at only three possible temperatures ( $-40$ ,  $-45$ , and  $-50^{\circ}$  C), dependent upon the ambient temperature. The dark level was typically  $< 1\%$  of the total background for observations taken at  $-50^{\circ}$  C and  $< 3\%$  for observations at  $-40^{\circ}$  C. Consequently, dark current was an important source of background in our images.

We constructed a master dark from thirty 5-minute dark exposures obtained in late

November taken at a CCD temperature of  $-50^{\circ}$  C. (The resulting error in photometry caused by using this dark frame with science frames obtained at the other temperatures was well below 1%.) The frames were combined using a median average and divided by the exposure time to yield a dark frame in counts per second. The dark frame multiplied by the exposure time was subtracted from each image.

### 2.3.2. Flat Field

The division of the flat field removes the pixel-to-pixel variations of the quantum efficiency. As with the dark frame, we used the same flat field for all images. This flat was constructed from about 12 individual twilight flat field frames taken around the same dates as the dark frames. No major changes to the telescope or the instrument configuration were made during the entire observing program. Nonetheless, we tested the flat obtained in November with a set of flats obtained at the end of the program. There was an average deviation between the two flats of 0.5% across the entire chip and a maximum deviation of about 3% close to the edges. Inspection of flat-fielded images did not show any prominent residual features attributable to an improper flat. However, to account for small flat field errors, we added an error of 0.005 mag in quadrature with the photometric errors.

### 2.3.3. Fringe Subtraction

Night sky emission lines can reflect several times inside a thinned CCD and cause interference. This interference is a source of coherent background in our science images and manifests itself as a fringe pattern present in the raw images. The pattern is stable but the amplitude of the fringes is highly variable and depend on moonlight, the exposure time, cloud cover, and position in the sky. Fringes are also an additive effect, unlike the multiplicative effect of the flat field. Since many of our targets are faint compared to the background, it is important that we correctly determine the pattern of the fringes and accurately compute the pattern's amplitude in the raw images.

Incidentally, there is no evidence of fringing in our twilight flats, presumably because the source of the light in the flats is scattered sun light. The flux from this scattered light dominates over the night sky lines responsible for the fringing in the science frames.

We assumed that the background of the images consisted of a normalized fringe frame representing the interference component multiplied by some image-dependent factor  $l_1$ , a constant continuum sky  $l_0$ , and brightness gradients along the X and Y axes scaled by  $l_2$

and  $l_3$ , respectively, to account for any moonlight or scattered light. After a frame was flat fielded and dark subtracted a mask was placed on the frame to remove all pixels  $5\sigma$  above the sky. The linear X and Y gradients were constructed and best fits to the factors  $l_0$ ,  $l_1$ ,  $l_2$ , and  $l_3$  were found for a  $300\times 300$  pixel box from the central region of the image. The normalized fringe frame was multiplied by  $l_1$  and subtracted from the image.

We constructed the normalized fringe frame from a large set ( $> 50$ ) of science frames that were either from different target fields or from fields in which the stars had been significantly offset. For a first guess at the fringe frame, we reduced the individual frames with the flat field and dark frame. Each frame was then divided by its sky level, creating a set of normalized frames. These frames were median averaged to form a fringe frame. The next iteration reduced the images with the dark, flat field, and the first guess at the fringe frame so that the four components of the background, most importantly  $l_0$  and  $l_1$ , could be found. Next, we reduced the raw frames again, this time using only the flat and dark. These frames were normalized by subtracting the sky continuum  $l_0$  and dividing by the fringe level  $l_1$ . They were then median averaged to create a new fringe frame. This process was iterated three more times, with each iteration using the fringe frame from the previous iteration. The final result was a fringe frame normalized to a mean value of 0.

This method for the fringe removal worked reasonably well, in the sense that in most frames the fringe patterns were completely removed. For the frames in which the fringes were not completely removed, the residual fringe level was significantly  $< 1\%$  the level of the background. We added an error term, discussed below, to account for sky subtraction errors from an imperfect fringe subtraction.

## 2.4. Photometry

We used aperture photometry to obtain the instrumental magnitudes of the targets and references. A circular aperture with a radius of 4 pixels was used to compute source fluxes; sky levels were determined from an annulus between 10 and 24 pixels from the source center. We performed differential photometry with the reference being the average brightness of non-variable stars in the field. Using a reference that is the average of many stars increased the signal-to-noise ratio in our target light curves. Furthermore, any color dependence on telluric extinction due to the difference in color between the targets and references was minimized by obtaining our science frames at low airmass (nearly 80% of our science frames were obtained at an airmass below 1.4 and 50% were below 1.24 airmasses).

During the reduction process some frames were thrown out because there was an obvious

problem with those frames. The most common problems were streaked stars due to tracking or guiding errors and missing stars from cloudy skies or an automatic dome closure. Frames with less obvious problems (e.g. being slightly out of focus) were allowed to go through the reduction process, but some were removed later as discussed below.

The first step in computing the mean reference is the determination of which reference stars are non-variable. Our ability to detect the variability of an object depends strongly on that object’s photometric errors. These errors are computed from the Poissonian error of the object, the sky noise error, and the error of the mean sky level, which is taken to be 0.15% of the mean sky value. We use this last term to account for errors in the fringe subtraction. We find that its use increases the photometric errors in all objects. The increase is largest for the fainter objects, allowing for a more conservative estimate of variability in these objects. We also add an error of 0.005 mag in quadrature with the photometric errors to account for changes in the flat field that occurred throughout the course of the observations. This additional error is a considerable fraction of the total error in the brightest objects and negligible in the faint ones. Consequently, its effect on the detection of variability is only important for the bright objects.

After all the data are collected for a target, the data set is put through several filters to remove bad points. The first processing filter removes all frames in which the average FWHM (full width at half maximum) of the stellar profiles is  $> 3''$ . This ensures that we do not use frames where the stars are slightly elongated, out of focus, or subject to poor seeing conditions. In general, these high FWHM frames have larger photometric errors.

The data for each reference star,  $k$ , is analyzed in a method similar to Bailer-Jones & Mundt (1999) to determine if the reference is stable and acceptable. This is accomplished by first computing the average flux for all references in frame  $j$ , excluding reference  $k$ , and converting it to a magnitude,

$$\overline{f_{kj}} = \frac{1}{n-1} \sum_{i=1, i \neq k}^n 10^{-0.4m_{ij}} \quad (1)$$

$$\overline{m_{kj}} = -2.5 \log(\overline{f_{kj}}), \quad (2)$$

where  $m_{ij}$  is the instrumental magnitude for reference  $i$  in frame  $j$ ,  $n$  is the number of references. The difference in magnitude between reference  $k$  and the mean reference is formed and  $\chi^2$  is computed in order to determine the probability that  $k$  is variable,

$$\Delta m_{kj} = m_{kj} - \overline{m_{kj}} \quad (3)$$



$$\chi_k^2 = \sum_{j=1}^N \left( \frac{\Delta m_{kj} - \overline{\Delta m_k}}{\sigma_{kj}} \right)^2, \quad (4)$$

where

$$\overline{\Delta m_k} = \frac{1}{N} \sum_{j=1}^N \Delta m_{kj}, \quad (5)$$

$N$  is the number of frames, and  $\sigma_{kj}$  is the photometric error associated with  $\Delta m_{kj}$ .

The  $\chi^2$  statistic is computed for each reference and the probability of variability ( $p$ ) for the reference with the largest  $\chi^2$  is calculated. If  $p > 95.4\%$  (a  $2\sigma$  detection), that reference is flagged as variable and removed from the list of references. This process of computing the mean reference and removing variable references is iterated until no more variable references are found. Finally, we calculate a mean reference for each frame based solely on the non-variable references.

Using all frames we compute the median brightness of the mean reference. We then remove any frame for which the brightness of the mean reference deviates by more than 0.5 mag from the median brightness. This effectively removes frames that are heavily obscured by terrestrial clouds.

Using this set of good frames, we re-analyze each reference (even the ones previously flagged as variable) and check for variability. As before the non-variable references are combined to make a mean reference for a given frame. In most cases the set of good references were the same before and after the removal of faint frames. Table 2 presents how many good references were found for each L-dwarf field.

### 3. Target Data Analysis

#### 3.1. Statistical Analysis

Differential magnitudes are computed for the target, using the mean reference as the reference “star.” The mean brightness of this differential light curve is found and a  $\chi^2$  test is used to determine how much the light curve deviates from a constant value centered on the mean. The value of  $\chi^2$  and the number of degrees of freedom in the computation of  $\chi^2$  are used to calculate the probability that  $\chi^2$  is obtained by chance. If this probability is  $< 0.046$  (i.e.  $p > 95.4\%$ , a  $2\sigma$  detection), then the target is flagged as variable. Targets suspected of being variable are searched for periodic variations using the method described below.

It is important to note  $\chi^2$  for an object and, consequently, the variability probabil-

ity, depend strongly on the estimate of that object’s errors. These errors are difficult to accurately determine and any changes to our estimate of the errors results in a change in  $\chi^2$ . Therefore, these results should be regarded as more of a gauge for variability than an absolute classification.

### 3.2. CLEAN Periodogram

A CLEAN periodogram routine (Roberts, Lehár, & Dreher 1987) is used to search for periods in the data of the suspected variable objects. This routine computes a “dirty” power spectrum, whose components consist of the spectrum of the frequency components convolved with the observing window function derived from the temporal sampling of the data. The power spectrum is “CLEANed” by subtracting the dominant peak convolved with the window function from the dirty spectrum to produce a residual spectrum. To aide in the stabilization of the routine, only a fraction, called the gain, of the response from the dominant period is removed. Next, the second highest peak (multiplied by the gain) is removed from the residual spectrum. Subsequent peaks are removed in the same fashion until all CLEAN components are obtained. This process is repeated for additional CLEANings. After a user–specified number of CLEANings are performed, the final spectrum is constructed based on the CLEAN components and the final residual spectrum. For consistency in our period computations we use a gain of 0.5 and 100 CLEANs for all variable targets.

The CLEAN routine removes most of the “problem” frequencies associated with the window function that are present in a Lomb-Scargle routine (Press et al. 1992). The result is a routine that is better able to find significant periods present in the data. The downside to this method is that there is no indicator for the noise in the power spectrum.

Bailer-Jones & Mundt (2001a) provide an algorithm for estimating the noise in a CLEAN power spectrum. This noise depends on the total amount of time in large gaps (we define a large gap as any time between points >12 hours) for the observing run. The amount of time attributed to large gaps was usually considerable for our runs and resulted in very small power spectrum noise values. Consequently, numerous peaks could occur in a given power spectrum that are several hundred times higher than the computed noise. This makes it difficult to establish which peaks are significant and which are meaningless.

To overcome this shortcoming, we attempt to estimate the noise by calculating the power expected for a synthetic data set with the same temporal sampling and RMS scatter as the real data set. The synthetic data set is created by randomly shuffling the magnitudes in the real data set to other times in the data set. The values of the magnitudes do not change,

only the time at which they occur. Any periodicity in the original data set is erased when the data are randomized. Therefore, the results of the CLEAN analysis for the synthetic data provide what powers can be expected for a set a random data with a certain RMS scatter. We take the mean value of the primary peak power from 1000 random shuffles as the noise level in the original data set. We calculate the primary peak power to noise ratio (PNR); data with periodic variations should have a PNR value several times greater than 1.

#### 4. Results

The variability results for our sample are presented in Table 2. Included are the total number of nights each object was observed and the number of nights in the final data set, the number of good images used in the analysis and the total taken, the number of days the data sets cover ( $t_{max}$ ), the number of good references used for the mean reference and the total number initially considered, the probability the L dwarf is variable ( $p$ ), the standard deviation of the points from the mean level ( $\sigma_{RMS}$ ), and the average error ( $\overline{\sigma_m}$ ).

We have already defined the variable L dwarfs as those with probabilities above 95.4%. This group constitutes 7 out of the sample of 18 targets. The five objects with  $p \sim 80\%$  are considered possibly variable, since they are likely to be viewed as variable with higher precision photometry. The six objects with  $p < 35\%$  clearly show no variability above the detection limits of this study.

Supporting of our claim for variability in the L dwarfs, Figure 1 shows the fraction of the total number of objects with a given probability of variability. Over 60% of the references have probabilities below 5%, whereas only 10% of the L dwarfs do. In addition, about 40% of the L dwarfs are flagged as variable ( $p > 95.4\%$ ) compared to about 15% for the references. Furthermore, Figure 2 shows the number of variable objects as a function of instrumental magnitude. The fraction of references in a given magnitude bin that are variable does not show any indication of being a strong function of object brightness, suggesting that we are not underestimating the errors in these objects. The slight increase between  $m_I=14-15$  in the references is likely due to small number statistics. Given this evidence, it seems clear that the L dwarfs derive from an inherently more variable population than the reference stars.

Three of the targets in our sample were also monitored by Bailer-Jones & Mundt (2001a): 2MASS 1146+22AB, 2MASS 1439+19, and 2MASS 0345+12. Our results disagree on the status of 2MASS 1146+22AB. This object is significantly non-variable in our sample, whereas Bailer-Jones & Mundt (2001a) detected variability with an RMS amplitude of 0.015 mag. Our average photometric error for this object is almost four times larger than this amplitude.

It is quite possible that 2MASS 1146+22AB varies with such a small amplitude as to be undetectable in this work. Therefore, even though we find that this object does not display statistically significant variations, higher signal-to-noise observations could show that it is still a low-amplitude variable.

The second object, 2MASS 1439+19, is classified as a possible variable here and a non-variable by Bailer-Jones & Mundt. Interestingly, their variability probability is larger than the one we find here (90% compared to 80%). Given that the probabilities are similarly high, this object is likely a low-amplitude variable.

We agree with the results of Bailer-Jones & Mundt (2001a) on the classification of 2MASS 0345+12 as a variable object. The light curve of 2MASS 0345+25 (Figure 3) shows quite a bit of scatter, but no periodic trends are evident. The primary peak in the CLEAN power spectrum occurs at  $24.1 \pm 0.1$  hours with a power  $\approx 8$  times higher than the noise. A couple of reference stars have prominent CLEAN peaks at 12 hours, indicating that the period is not intrinsic to any one object. Consequently, we list 2MASS 0345+25 as a variable object in Table 2, but do not present it in Table 3.

Gelino, Marley, & Holtzman (2001) presented preliminary results for three L dwarfs in this program. They found 2MASS 0036+18 and 2MASS 0135+12 to be variable and 2MASS 1412+16 to be non-variable. An error was found in the reduction process used to obtain those results. The FWHM used to reject high FWHM frames was only from one star, and not an average of all stars. Upon correction of the error, the classification of 2MASS 0036+18 changed from variable to non-variable. The classifications of the other two objects did not change, but their data sets did change slightly. The new light curve for 2MASS 0135+12 is shown in (Figure 4). This object does not have a significant period (Table 3), contrary to what was reported previously.

2MASS 1108+68 is another L dwarf displaying statistically significant variations and no significant period. With a baseline of nearly 6 months (Figure 5), the data obtained for this object represents the most extensive photometric monitoring of any L dwarf to date.

Though not as extensive as 2MASS 1108+68, 2MASS 0746+20AB also has very good coverage (Figure 6). This binary is the brightest object in our target list and is variable. The most dominant peak in the CLEAN power spectrum (Figure 7) is quite high compared to other peaks and is present at a period of  $31.0 \pm 0.1$  hours. The power of this period is nearly 5 times higher than the noise and the phased data (Figure 8) shows a roughly sinusoidal light curve.

Basri et al. (2000) present  $v \sin i$  measurements for twelve L dwarfs, including 2MASS 1439+19 and 2MASS 1146+22AB from this study. The values they derive span from  $10 \pm 2.5$

to  $60 \pm 5 \text{ km s}^{-1}$ . For typical brown dwarf radii (Burrows et al. 1997), these velocities translate to rotation periods  $\lesssim 10$  hours. Because the inclination angle of the rotation axis is unknown, this period is an *upper* limit to the true rotation period of these objects. Consequently, the 31-hour period found here is likely too long to be related to the rotation period.

The first 70 days of coverage for 2MASS 0746+20AB reveal an interesting trend (Figure 9). The data appear to have a rough saw-tooth light curve that repeat with a period of approximately 20 days. After HJD 1950 this pattern is not as prominent. It is unclear what variability source can cause a saw-tooth pattern such as this. Spots and clouds should produce more gradual changes in the light curve. A flare would produce a sudden brightening, followed by a gradual dimming, the opposite to what is seen here. Furthermore, Reid et al. (2001) estimate an orbital semi-major axis of 3.4 AU, giving a period of about 18 years. Therefore, both the shape and duration of the feature are not what would be expected for an eclipsing system.

2MASS 1300+19 also has an interesting feature in its light curve (Figure 10). The sequence of points around HJD=2027 (Figure 11) show roughly sinusoidal variations. This span of points is approximately the same as the best period for the entire data set, 238 hours, indicating that this feature is the source of the period. The period is much longer than expected for a rotation period. It seems likely that some other cause is responsible for the feature.

Although the feature is reminiscent of an eclipsing binary light curve, this scenario seems unlikely. The depth of the feature implies a secondary object radius about 18% the radius of the L dwarf, roughly 3 times larger than Earth. The duration suggests an orbital separation  $> 500$  AU. The probability that we should observe an edge-on binary system with an orbital separation  $> 500$  AU just as it is eclipsing is extremely small ( $< 10^{-7}$ ). Furthermore, while there are stars with L and T dwarf companions at separations greater than 500 AU, there are no known companions to L dwarfs beyond 10 AU.

It is possible that the 10-day feature in this object’s light curve is related only to its surface features. The sudden creation and dissipation of a large storm could possibly produce the changes we see. A similar event happened with Saturn several years ago (Beebe et al. 1992), but over a longer dissipation timescale. However, features on Jupiter and Saturn are known to evolve on timescales from hours to years, depending on the features’ positions and rotation orientations (Beebe 2001, private communication), so the timescale seen here is certainly plausible. A large storm would not only change the brightness of the object, it should also have an effect on the photometric colors.

Table 3 presents the primary CLEAN periods and their PNR for six variable and five

possibly variable L dwarfs. The only periods considered significant are those with PNR values above 3, 2MASS 0746+20AB and 2MASS 1300+19. We have discussed why we do not believe these periods to be related to the rotation period of these objects.

In addition to the objects mentioned above, our sample contains several other objects (Table 2). These objects do not have significant periods, nor do they have any interesting features in their light curves. The light curves for all objects will be found in Gelino (2002).

## 5. Possible Variability Sources

We have discussed the existence of statistically significant photometric variations in seven of eighteen L dwarfs and possible variations in another five. These variable objects cover the entire span of spectral types present in our sample, from L0 to L4.5. Their data were sampled with a minimum timescale of  $\sim 5$  minutes, intra-night sampling  $\sim 1$ -2 hours, and maximum baselines between 26 and 230 days. Most of these variables show no significant periodicity. Whatever the source of these variations, it must be present in a variety of spectral types and, hence, effective temperatures.

Two properties are commonly mentioned in the literature in which L dwarfs can be unusual:  $H\alpha$  and variability. These may or may not be related since some of the variable L dwarfs have  $H\alpha$  present in their spectra and others do not. We now discuss possible sources for the variations and their likelihood of being present in these objects.

### 5.1. Magnetic Spots

#### 5.1.1. Summary of Magnetic Activity Observations

Many L dwarfs exhibit  $H\alpha$  emission (Kirkpatrick et al. 1999, 2000), which is known to be an indicator of high chromospheric temperatures and magnetic activity in earlier type stars (Hawley et al. 2000). If the variability in L dwarfs is caused by magnetic spots, then it is plausible to expect a correlation between  $H\alpha$  emission and the variable objects. In agreement with the conclusions of (Bailer-Jones & Mundt 2001a) and (Martín et al. 2001), Figure 12 shows no correlation between  $H\alpha$  emission (i.e. magnetic activity) and variability for the sample of L dwarfs from (Bailer-Jones & Mundt 2001a) and this study. This result could imply that either magnetic activity is not the source of the variation or that the  $H\alpha$  emission is not magnetic in origin for these objects.

As with earlier-type stars, wave heating has been suggested as the mechanism responsi-

ble for producing hot brown dwarf upper atmospheres (Yelle 2000). Convection-forced waves propagate and grow as they rise through the upper atmosphere, eventually releasing their energy and heating the gas as they dissipate. The resulting high temperatures combined with magnetic field effects are possibly responsible for the  $H\alpha$  emission. L dwarfs with weak magnetic fields should exhibit little or no  $H\alpha$  emission. In light of this it is quite notable that the fraction of objects with  $H\alpha$  emission peaks at spectral type M7 and decreases at earlier and later spectral types (Gizis et al. 2000). No L dwarfs later than L5 show  $H\alpha$  in emission (Kirkpatrick et al. 2001), although one T dwarf does (Burgasser et al. 2000). Since the early L population consists of both young brown dwarfs and old stars, this trend could indicate an inability of either substellar objects or cool stars to produce magnetic fields appropriate to maintain the  $H\alpha$  emission (Gizis et al. 2000).

Using kinematics as a probe for age, Gizis et al. (2000) have argued that the substellar late-type dwarfs show less  $H\alpha$  emission than stellar dwarfs of the same effective temperature. This might imply that the process by which  $H\alpha$  emission is produced is driven by the mass of the object and not the effective temperature. Indeed, the dissipation of acoustic waves in the upper atmosphere could be responsible for the heating of the chromosphere. Unfortunately, this process is poorly characterized at the masses and effective temperatures of interest here.

In addition to  $H\alpha$  emission, radio emission can also be a signature of a magnetic field. Radio flares as well as quiescent emission have recently been reported for the M-dwarfs LP944–20 (Berger et al. 2001) and BRI0021 (Berger 2002), and the L3.5 dwarf 2MASS 0036+18 (Berger 2002), an object in our sample. These authors infer that the radio emission is caused by synchrotron emission and estimate field strengths of  $\sim 5$  G for LP944–20, 5-50 G for BRI0021 and 20-350 G for 2MASS 0036+18. Since there are essentially no methods to accurately determine the magnetic field strengths of objects other than the sun (Haisch, Strong, & Rodono 1991), these values are based upon models and assumptions that might not be correct. Regardless of these assumptions, however, Berger (2002) surmises that this data imply a substantial, non-neutral corona in this L dwarf, although the mechanics to create such a corona are poorly understood.

If the magnetic field strengths are correct for LP944–20, BRI0021, and 2MASS 0036+18, they are apparently much less than the field strengths of active M dwarfs (Haisch et al. 1991). In addition, the substellar nature, old age (Tinney 1998), and rapid rotation (Tinney & Reid 1998) of LP944–20 support a weak field strength; many L dwarfs with spectroscopically determined rotation velocities are rotating quite rapidly and lack significant  $H\alpha$  emission (Hawley et al. 2000), suggesting that the magnetic fields of these presumably old objects are too weak to slow down the rotation. The rotation velocity of 2MASS 0036+18 is unknown and it has no measurable  $H\alpha$  emission.

The existence of a magnetic field in LP944–20 is also supported by the observation of an X-ray flare (Rutledge et al. 2000). An X-ray flare in an old, non-accreting object such as this can only be caused by magnetic activity. However, the lack of quiescent X-ray emission suggests that the magnetic field is quite weak. Rutledge et al. postulate that because of the rapid rotation in this object, either the turbulent dynamo is being suppressed or the magnetic field is being configured into a more organized form. They also suggest that the lack of ionization in the cool photosphere prevents the magnetic field from coupling with the gas in the atmosphere, causing the field to dissipate.

Fleming, Giampapa, & Schmitt (2000) arrive at the same conclusion with their study of the X-ray flare of the M8 dwarf VB 10. They go so far as to estimate the ionization fraction in its atmosphere, by extrapolating the ionization fractions in the atmospheres of early dwarfs down to the effective temperature of VB 10. They estimate that the ionization fraction in late M dwarfs is 2 orders of magnitude lower than in early M dwarfs and 3 orders of magnitude smaller than in the sun, and conclude that magnetic footprints (i.e. spots) are unlikely to exist in the photosphere. The cooler M9 dwarf LP944–20 is even less likely to have magnetic spots than VB 10, supporting the conclusion by Tinney & Tolley (1999) that they were detecting the signature of clouds. This, in turn, implies that magnetically produced spots are unlikely to be found in L dwarfs. However, it is still useful to examine what conditions are needed for the formation of magnetic spots and to determine if these conditions exist in L dwarfs.

### 5.1.2. *Model Predictions*

Magnetic spots in the sun (i.e. sunspots) are thought to form as magnetic flux tubes rise to the photosphere (Parker 1955). For magnetic buoyancy to be important, the plasma must be a sufficiently good conductor. This criterion is most likely not satisfied in cool L-dwarf atmospheres, especially in the low pressure regions where the temperatures are also low. In these regions the free electron abundance is small,  $\sim 10^{11} \text{ cm}^{-3}$  around 1 bar for a 2000 K model. While this density is only an order of magnitude less than coronal densities estimated by Berger (2002), it is a factor of  $10^7$  smaller than the densities of neutral species (e.g.  $\text{H}_2$ , and He) at this atmospheric pressure. The corona is likely a low-density region populated primarily by free electrons, whereas the atmosphere at a pressure of 1 bar is largely neutral. Therefore, these two regions should have substantially different electrical conductivities. The small fraction of free electrons relative to neutral species in the atmosphere suggests that this region should not be a good conductor, nor should it be able to support the formation of any magnetic spots. Nonetheless, it is instructive to explore the possibility of magnetic



spots in more detail.

To estimate the strength of coupling between the gas and the magnetic field we compute the magnetic Reynolds number  $R_m$  for L-dwarf atmospheres.  $R_m$  is a dimensionless parameter describing how efficiently a gas interacts with a magnetic field;  $R_m = lv/\eta$  (Priest 1982), where  $l$  is a length scale,  $v$  is a velocity scale, and  $\eta$  is the magnetic diffusivity of the gas. When  $R_m \ll 1$ , the magnetic field slips through the gas with no interaction; for  $R_m \gg 1$ , the magnetic field is frozen in the gas.

To compute  $R_m$  we rely on atmosphere models computed by Marley et al. (2002) for cloudy L dwarfs. The models employ the cloud model of Ackerman & Marley (2001) with the best-fitting sedimentation parameter  $f_{\text{rain}} = 3$ . The L-dwarf  $T_{\text{eff}}$  range is still uncertain, but likely lies between about 2200 and 1300 K. We consider models with  $T_{\text{eff}}$  of 2000 to 1200 K and surface gravity of  $10^5 \text{ cm s}^{-2}$ , appropriate for a  $\sim 35$  Jupiter mass brown dwarf.

The appropriate length scale  $l$  to use in the calculation of  $R_m$  is not obvious. In the area around sunspots,  $l$  is usually taken as the size of the sunspot, a small fraction of the solar radius. We choose to set  $l = H$ , the pressure scale height. Typical values of  $H$  are around  $10^6 \text{ cm}$  at the 1 bar level. For the velocity scale we use that predicted by mixing length theory. To place a conservative upper limit on  $v$  and hence  $R_m$ , we assume that the entire thermal flux of the L dwarf is carried by convection. This is reasonably accurate below the photosphere, but overestimates the velocity scale, and  $R_m$ , above. Typical convective velocities are computed to be  $10^3\text{-}10^4 \text{ cm s}^{-1}$ .

The value for  $\eta$  is computed from Priest (1982);

$$\eta = 5.2 \times 10^{11} \ln \Lambda T^{-3/2} A \text{ cm}^2 \text{ s}^{-1}, \quad (6)$$

where

$$A \approx 1 + 5.2 \times 10^{-11} \frac{n_n T^2}{n_e \ln \Lambda} \quad (7)$$

is a factor to account for the partial ionization of the plasma,  $T$  is temperature,  $n_n$  is the number density of neutral atoms and molecules,  $n_e$  is the number density of electrons, and

$$\ln \Lambda \approx \ln \left( 1.24 \times 10^4 \frac{T^{3/2}}{n_e^{1/2}} \right) \text{ for } T < 5.8 \times 10^5 \text{ K} \quad (8)$$

is the Coulomb logarithm (Somov 1992). We use the abundance tables of Lodders (1999) to calculate  $n_e$  and  $n_n$ . At a pressure of 1 bar  $n_n$  is  $\sim 10^{18} \text{ cm}^{-3}$  for all models, whereas values of  $n_e$  at this level are  $\sim 10^7 \text{ cm}^{-3}$  for the 1200 K model and  $\sim 10^{11} \text{ cm}^{-3}$  for the 2000 K model.

Equation 8 provides a useful relation for computing the Coulomb logarithm at temperatures below  $10^6$  K. This relation might not be valid in the atmospheres of L dwarfs, where the temperatures of interest here do not exceed 4100 K. For a given model,  $\ln \Lambda$  as calculated above varies between 5 and 30 throughout the atmosphere. In order to test the validity of these results, we computed  $R_m$  with  $\ln \Lambda$  at the unrealistic values of 1 and 100. We find that  $R_m$  computed at these limits differs by less than 1 part in  $10^6$  for our coolest model and  $< 1\%$  for our warmest model and stress that for the region of parameter space covered by our calculation the precise value of  $\ln \Lambda$  is essentially irrelevant. Nonetheless, for the results considered here,  $\ln \Lambda$  is computed with Equation 8.

The value of  $R_m$  as a function of pressure in the model atmospheres is shown in Figure 13.  $R_m$  is very small throughout the entire upper atmosphere; only at pressures of  $\sim 100$  bar and higher does  $R_m$  start to approach 1. By comparison,  $R_m$  near sunspots is estimated to be  $10^4$ - $10^6$  (Priest 1982). Open circles denote the approximate base of the photosphere (where  $T = T_{\text{eff}}$ ) for the models shown. Note that in contrast to the sun,  $R_m$  only approaches unity well below the photosphere. At  $R_m=1$ , the plasma and the magnetic field will interact with each other only to a small degree. Any weak magnetic disturbances deep in these atmospheres are unlikely to affect the surface thermal flux since the winds and weather patterns alluded to earlier will redistribute the upwelling thermal flux before it is radiated. Thus, throughout the atmospheres of L dwarfs, spanning the range from roughly L2 to L8 (Kirkpatrick et al. 1999, 2000) we expect little or no interaction between the visible atmosphere and the magnetic field.

As mentioned above, the choice of  $l$  and  $v$  are not obvious. It is easy to imagine the use of other values, both larger and smaller, for these parameters. Larger values would increase  $R_m$  and smaller values would, of course, decrease it. Nonetheless, the values used here are reasonable and meant only to estimate  $R_m$ .

It is also important to note that we have made no assumptions regarding how magnetic fields in L dwarfs are made or sustained. Despite our comparisons to the sun, there is no reason to expect a magnetic field in an L dwarf to be created in the same method as the field in the sun. Indeed, the origin of the magnetic field is irrelevant to the calculation above, since it is the characteristics of the gas that regulate the degree of coupling.

## 5.2. Clouds

The thermal fluxes emerging from L-dwarf atmospheres are affected by clouds. Early L dwarfs have relatively thin clouds high in the atmosphere (Ackerman & Marley 2001).

Figure 13 illustrates the trend for the clouds to form progressively deeper in the atmosphere at later spectral types. The base of the photosphere is marked for the models shown. Unlike the case for  $R_m$  approaching unity, the clouds form in the immediate vicinity of the photosphere and thus are well placed to affect the emitted thermal flux. For objects with  $T_{\text{eff}} \leq 2000\text{K}$  (approximately L2 and cooler; Stephens et al. 2001) clouds play an important role in the emitted flux since the condensate opacity is significant.

For an arbitrary L dwarf the emitted flux in some spectral regions will be limited by the cloud deck, while in others gaseous opacity reaches optical depth unity above the cloud. Marley et al. (2002) illustrate the effects of gaseous and condensate opacity for a variety of L dwarfs. If there is a transitory clearing in the cloud deck additional flux will emerge from those spectral regions in which the cloud opacity is otherwise dominant. Examples are the peaks of flux emerging from the water band windows in  $z$ ,  $J$ ,  $H$ , and  $K$  bands and the optical flux in  $I$  band. The resulting bright spots on the objects will be similar to the ‘5- $\mu\text{m}$  hot spots’ of Jupiter (Westphal, Matthews, & Terrile 1974) where flux emerges from holes in the ammonia cloud. An atmosphere with such non-uniformly distributed high contrast regions should be quite capable of producing photometric variations.

As cloud optical thickness increases with later spectral type, L-dwarf  $J - K_s$  color becomes redder, eventually saturating around 2 (Marley 2000; Allard et al. 2001; Ackerman & Marley 2001; Marley et al. 2002; Tsuji 2001). Clouds in cooler objects lie well below the photosphere, and leave the radiating region in the atmosphere relatively clear. The clear atmosphere partially manifests itself in the blue  $J - K_s$  seen in the T dwarfs (Allard et al. 1996; Marley et al. 1996; Tsuji et al. 1996).

Models predict (Marley 2000; Marley et al. 2002; Burgasser et al. 2002) that a hypothetical L dwarf with no clouds will be substantially bluer ( $\sim 1.5$  mag; Marley & Ackerman 2001) at  $J - K_s$  than a more realistic object with the same effective temperature and a cloudy atmosphere. Thus, if the average L dwarf at a given spectral type is entirely covered with clouds, it would not likely be seen as a variable and it would have more typical  $J - K_s$  color. In order for photometric variations to arise by the cloud mechanism there must be non-uniformity in the cloud coverage, such as clearings in the clouds. So, not only would clear sections of the atmosphere (holes) provide a source for brightness variations, flux emerging through such holes would cause the  $J - K_s$  color to be somewhat bluer than the average object. The lack of a similar trend for the early L and late M dwarfs might indicate a different mechanism is at work in those atmospheres. Of course variability caused by thicker clouds would result in variable objects being redder in  $J - K_s$  than non-variable objects.

Time-resolved multicolor photometry should be sufficient to determine if variability is

indeed connected to color. In the absence of such observations, we examine the previously published  $J - K_s$  colors in search of systematic differences between variable and non-variable L dwarfs. Figure 14 shows that there is no distinct difference between the variable and non-variable targets. Incidentally, plots using  $J - H$  and  $H - K_s$  also fail to reveal any significant trends (Gelino 2002). Perhaps this indicates that the cloud features producing the variations are not as simple as a single, isolated spot.

Schubert & Zhang (2000) argue that the atmospheres of L dwarfs likely exist in one of two states, chaotic or banded. Since clouds respond to atmospheric motions, they would presumably reflect one of these two morphologies. In general, Schubert & Zhang expect higher mass objects to have more chaotic and three-dimensional internal dynamics than lower mass objects, meaning that the higher mass objects are less likely to have banded cloud features. It is not obvious which cloud morphology would better produce photometric variations. For this reason, it is useful to speculate on what effects different cloud morphologies can have on an object’s photometry.

Objects with more chaotic atmospheres, for example, might be more likely to have uniformly distributed clouds. When rotating, such objects might show little photometric variation, unless chaotic motion produces rapid evolution of the clouds. If the chaotic atmospheres result in fairly complete cloud coverage, then we might expect that more massive L dwarfs would be redder in  $J - K_s$  and tend not to be variable. Conversely, if chaotic atmospheres more often produce large clearings in the clouds, then they may more easily produce photometric signatures than banded atmospheres. In this scenario, the more massive L dwarfs would be bluer in  $J - K_s$  and tend to be variable. Furthermore, rapidly evolving, chaotic atmospheres may be responsible for the changes in photometric period observed for some objects. It is easy to imagine similar scenarios for banded clouds. The lack of any trends with color for the few L dwarfs observed for variability could indicate that a variety of cloud morphologies are present in these objects. Clearly, more observations and modeling are required to better characterize atmospheric circulation and weather in L-dwarf atmospheres.

## 6. Discussion

The presence of clouds can explain the different types of variability seen in L dwarfs: non-variable, non-periodic variable, and periodic variable. The non-variable L dwarfs could be those objects whose atmospheres are either completely covered with clouds or whose clouds are uniformly distributed in spots and bands. Such cloud morphologies result in small photometric variations below our detection limit.

For an object to be classified as a periodic variable it must have some large feature that produces photometric variations and is stable, both temporally and spatially, over the entire span of the observations. None of the variable L dwarfs exhibit any periodic variations that lasted the entire program, suggesting that these conditions are not satisfied simultaneously in these objects. For example, a large storm could migrate latitudinally or dissipate and reform at a different latitude as does the Great Dark Spot in the atmosphere of Neptune (Hammel & Lockwood 1997). If wind speed is a function of latitude as on all the giant planets of our solar system, then spots at different latitudes will circle the object with different periods.

If the migrations or dissipations occur on timescales much shorter than the baselines of our observations, then we would not be able to find any periodic signal. On the other hand, if the evolutionary timescales are a significant fraction of the baseline, then a prominent feature should produce a temporary signal, though not necessarily periodic. Only two objects possibly fall under the latter category, 2MASS 0746+20AB and 2MASS 1300+19. They show features changing on timescales about 10 days and longer. The shortest baseline for the other variable objects is around 25 days. Any evolution of clouds in their atmospheres must occur on timescales shorter than this. Indeed, Bailer-Jones & Mundt (2001a) conclude that features they observe must evolve on timescales shorter than their maximum observing duration of around 5 days.

If an L dwarf has several large features at different latitudes, the photometric variations produced could be non-periodic. As mentioned above, an L dwarf is possibly a differentially rotating object. Features located at different latitudes may respond to different wind speeds, resulting in different rotation periods around the object. The resulting light curve would be a complex composite of several periodic signals with different amplitudes, periods, and phases. Photometric “noise” from smaller cloud features would degrade the periodic signals further, essentially making them undetectable. Since most of the light curves for the objects studied here have data randomly scattered about a mean value, it is likely that the atmospheres for these objects are non-uniformly covered with clouds and do not have any single dominant feature.

## 7. Conclusions

We have conducted a photometric monitoring program of eighteen L dwarfs in the  $I_C$  photometric filter. We find that seven of these eighteen display statistically significant variations above the 95.4% probability level and with RMS scatter between 0.010 and 0.083 mag. An additional five objects have probabilities for variability  $\approx 80\%$ , suggesting that these objects are possibly variable. The remaining targets have probabilities  $< 35\%$ , indicating that

they are non-variable or have amplitudes below our detectability.

Only three variable L dwarfs have prominent periods in their CLEAN power spectra that have power  $>3$  times the noise. The 24.1-hour period of 2MASS 0345+25 is not intrinsic to the L dwarf and needs more investigation. 2MASS 1300+19 has a 9-day section of its light curve that could be evidence for the creation and dissipation of a large storm. The source of the 31.0-hour period of 2MASS 0746+20AB is not clear from the light curve. However, it does have a 70-day section with a puzzling saw-tooth pattern with properties unlike any that would be expected. All of these timescales are much longer than the rotation periods expected for these objects.

The light curves of the other variable objects are quite random and have no dominant features. Non-uniform cloud coverage with features evolving on timescales less than a few days is likely the source of the variations in these objects. Indeed, we have shown that the low ionization fraction predicted by L-dwarf models and the accompanying low magnetic Reynolds numbers strongly argue against magnetic spots as a plausible cause for the photometric variations. On the other hand silicate and iron grains condense in L-dwarf atmospheres within the photosphere. These clouds are likely responsible for the photometric variations discovered in the various studies, particularly for the later L dwarfs (about L2 and later). Since the thermal emission of T dwarfs is also influenced by clouds (Marley et al. 2002) we predict that variability will also be found in the opacity window regions of these objects. Further work with models and more observations are required to better understand cloud composition and dynamics.

The authors wish to thank D.H. Roberts, J. Peterson, and B. Goldman for various contributions and discussions. We also wish to acknowledge the useful comments of the referee. C.G. and M.M. acknowledge support from NASA grants NAG2-6007 and NAG5-8919 and NSF grants AST-9624878 and AST-0086288. Work by K.L. supported by NSF grant AST-0086487.

## REFERENCES

- Ackerman, A. S., & Marley, M. S. 2001, *ApJ*, 556, 872
- Allard, F., Hauschildt, P. H., Baraffe, I., & Chabrier, G. 1996, *ApJ*, 465, L123
- Allard, F., Hauschildt, P. H., Alexander, D. R., Tamanai, A., & Schweitzer, A. 2001, *ApJ*, 556, 357

- Bailer-Jones, C. A. L. & Mundt, R. 1999, *A&A*, 348, 800
- Bailer-Jones, C. A. L. & Mundt, R. 2001, *A&A*, 367, 218
- Bailer-Jones, C. A. L. & Mundt, R. 2001, *A&A*, 374, 1071
- Basri, G., et al. 2000, *ApJ*, 538, 363
- Beebe, R. F., Barnet, C., Sada, P. V., & Murrell, A. S., *Icarus*, 95, 163
- Berger, E. 2002, *ApJ* in press (astro-ph/0111317)
- Berger, E., et al. 2001, *Nature*, 410, 338
- Bondar, N. I. 1995, *A&AS*, 111, 259
- Burgasser, A. J., Kirkpatrick, J. D., Reid, I. N., Liebert, J., Gizis, J. E., & Brown, M. E. 2000, *AJ*, 120, 1100
- Burgasser et al. 2002, *ApJL*, in press (astro-ph/0205051)
- Burrows, A., et al. 1997, *ApJ*, 491, 856
- Burrows, A., & Sharp, C. M. 1999, *ApJ*, 512, 843
- Clarke, F. J., Tinney, C. G., & Covey, K. R., *MNRAS*, 332, 361
- Fleming, T. A., Giampapa, M. S., & Schmitt, J. H. M. M. 2000, *ApJ*, 533, 372
- Gelino, C. R. 2002, Ph.D. Dissertation, in preparation
- Gelino, C. R., & Marley, M. S. 2000, in *ASP Conf. Ser. 212, From Giant Planet to Cool Stars*, ed. C. A. Griffith & M. S. Marley (San Francisco: ASP), 322
- Gelino, C. R., Marley, M. S., & Holtzman, J. A. 2001, to appear in the *Proceedings of the 12th Cambridge Workshop on Cool Stars, Stellar Systems, and the Sun*
- Gizis, J. E., Monet, D. G., Reid, I. N., Kirkpatrick, J. D., Liebert, J., & Williams, R. J. 2000, *AJ*, 120, 1085
- Haisch, B., Strong, K. T., & Rodono, M. 1991, *ARA&A*, 29, 275
- Hammel, H. B., & Lockwood, G. W. 1997, *Icarus*, 129, 466
- Hawley, S. L., Reid, I. N., & Gizis, J. E. 2000, in *ASP Conf. Ser. 212, From Giant Planets to Cool Stars*, ed. C. A. Griffith & M. S. Marley (San Francisco: ASP), 252

- Johns-Krull, C. M., & Valenti, J. A. 1996, *ApJ*, 459, L95
- Kirkpatrick, J. D., et al. 1999, *ApJ*, 519, 802
- Kirkpatrick, J. D., et al. 2000, *AJ*, 120, 447
- Kirkpatrick, J. D., Dahn, C. C., Monet, D. G., Reid, I. N., Gizis, J. E., Liebert, J., & Burgasser, A. J. 2001, *AJ*, 121, 3235
- Koerner, D. W., Kirkpatrick, J. D., McElwain, M. W., & Bonaventura, N. R. 1999, *ApJ*, 526, L25
- Lodders, K. 1999, *ApJ*, 519, 793
- Marley, M. S. 2000, in *ASP Conf. Ser. 212, From Giant Planets to Cool Stars*, ed. C. A. Griffith & M. S. Marley (San Francisco: ASP), 152
- Marley, M. S., & Ackerman, A. S. 2001, proceedings of IAU Symposium 202, “Planetary Systems in the Universe: Observation, Formation and Evolution” in press ([astro-ph/0103269](http://astro-ph/0103269))
- Marley, M. S., Saumon, D., Guillot, T., Freedman, R. S., Hubbard, W. B., Burrows, A., & Lunine, J. I. 1996, *Science*, 272, 1919
- Marley, M. S., Seager, S., Saumon, D., Lodders, K., Ackerman, A. S., Freedman, R. , & Fan, X. 2002, *ApJ*, 568, 335
- Martín, E. L., Delfosse, X., Basri, G., Goldman, B., Forveille, T., & Zapatero Osorio, M. R. 1999, *AJ*, 118, 2466
- Martín, E. L., Zapatero Osorio, M. R., & Lehto, H. J. 2001, *ApJ*, 557, 822
- Monet, D. et al. 1998, *USNO-SA2.0*, (U.S. Naval Observatory, Washington DC)
- Parker, E. N. 1955, *ApJ*, 121, 491
- Press, W. H., Teukolsky, S. A., Vetterling, W. T., & Flannery, B. P. 1992. *Numerical Recipes in Fortran 77: The Art of Scientific Computing* (2d ed; Cambridge: Cambridge University Press)
- Priest, E. R. 1982, *Solar Magnetohydrodynamics* (Dordrecht, Holland: D. Reidel Publishing)
- Reid, I. N., et al. 1999, *ApJ*, 521, 613
- Reid, I. N., Gizis, J. E., Kirkpatrick, J. D., & Koerner, D. W. 2001, *AJ*, 121, 489



- Reid, I. N., Kirkpatrick, J. D., Gizis, J. E., Dahn, C. C., Monet, D. G., Williams, R. J., Libert, J., & Burgasser, A. J. 2000, *AJ*, 119, 369
- Roberts, D. H., Lehár, J., & Dreher, J. W. 1987, *AJ*, 93, 968
- Rutledge, R. E., Basri, G., Martín, E. L., & Bildsten, L. 2000, *ApJ*, 538, L141
- Saar, S. H. 1994, in *IAU Symp. 154, Infrared Solar Physics*, ed. D. M. Rabin et al. (Dordrecht: Kluwer), 493
- Schubert, G., & Zhang, K. 2000, in *ASP Conf. Ser. 212, From Giant Planets to Cool Stars*, ed. C. A. Griffith & M. S. Marley (San Francisco: ASP), 210
- Somov, B. V. 1992, *Physical Processes in Solar Flares* (Dordrecht, Holland: Kluwer Academic Publishers)
- Stephens, D., Marley, M., Noll, K., & Chanover, N. 2001, *ApJ*, 556, L97
- Tinney, C. G. 1998, *MNRAS*, 296, L42
- Tinney, C. G., & Reid, I. N. 1998, *MNRAS*, 301, 1031
- Tinney, C. G., & Tolley, A. J. 1999, *MNRAS*, 304, 119
- Tsuji, T. 2001, *Proceedings of the IAU Workshop on “Ultracool Dwarfs: Surveys, Properties and Spectral Classification”* ed. H. R. A. Jones & I. Steele, in press
- Tsuji, T., Ohnaka, K., Aoki, W., & Nakajima, T. 1996, *A&A*, 308, L29
- Westphal, J. A., Matthews, K., & Terrile, R. J. 1974, *ApJ*, 188, L111
- Yelle, R. V. 2000, in *ASP Conf. Ser. 212, From Giant Planets to Cool Stars*, ed. C. A. Griffith & M. S. Marley (San Francisco: ASP), 267

Table 1. L Dwarfs Observed for Variability

Name	Spectral Type	R.A. J(2000)	Dec. J(2000)	$I$ Magnitude <sup>a</sup>	H $\alpha$ Emission <sup>b</sup>	Reference
2MASS 0015+35	L2	00:15:44.7	+35:16:03	$\sim 17.2$	Y	1
2MASS 0036+18	L3.5	00:36:15.9	+18:21:10	16.10	...	1,2
2MASS 0058–06	L0	00:58:42.5	–06:51:23	$\sim 17.5$	Y	1
2MASS 0135+12	L1.5	01:35:35.8	+12:05:22	$\sim 17.7$	Y	1
2MASS 0345+25	L0	03:45:43.2	+25:40:23	16.98	...	3
2MASS 0746+20AB	L0.5	07:46:42.5	+20:00:32	15.11	Y	1,2
2MASS 1029+16	L2.5	10:29:21.6	+16:26:52	$\sim 17.6$	Y	1
2MASS 1108+68	L1	11:08:30.7	+68:30:17	$\sim 16.6$	Y	4
2MASS 1146+22AB	L3	11:46:34.5	+22:30:53	17.62	...	3
2MASS 1300+19	L1	13:00:42.5	+19:12:35	$\sim 15.9$	...	4
2MASS 1338+41	L2.5	13:38:26.1	+41:40:34	$\sim 17.6$	...	1
2MASS 1411+39	L1.5	14:11:17.5	+39:36:36	$\sim 17.9$	...	1
2MASS 1412+16	L0.5	14:12:24.4	+16:33:12	$\sim 17.1$	Y	1
2MASS 1439+19	L1	14:39:28.4	+19:29:15	16.02	...	2,3
2MASS 1506+13	L3	15:06:54.4	+13:21:06	$\sim 16.9$	Y	4
2MASS 1615+35	L3	16:15:44.1	+35:59:00	$\sim 18.1$	...	1
2MASS 1658+70	L1	16:58:03.7	+70:27:01	$\sim 16.7$	...	4
2MASS 2224–01	L4.5	22:24:43.8	–01:58:52	$\sim 18.0$	Y	1

<sup>a</sup>Approximate magnitudes are estimated from the  $I - J$  color and the instrumental magnitudes.

<sup>b</sup>All targets have been observed for H $\alpha$  emission. Those entries listed as ‘Y’ have had definite detections; entries listed as ‘...’ indicate that only upper limits for emission have been obtained.

References. — (1) Kirkpatrick et al. 2000; (2) Reid et al. 2000; (3) Kirkpatrick et al. 1999; (4) Gizis et al. 2000

Table 2. L-Dwarf Variability Results

Name	Nights Used/Total	Frames Used/Total	$t_{max}$ [days]	References Used/Total	$p$ [%]	$\sigma_{RMS}$ [mag]	$\overline{\sigma}_m$ [mag]
2MASS 0345+25 <sup>a</sup>	35/37	209/318	108.73	7/7	>99.99	0.030	0.027
2MASS 0746+20AB	38/45	260/421	150.88	10/12	>99.99	0.010	0.007
2MASS 1300+19	37/39	275/384	137.78	5/7	>99.99	0.015	0.012
2MASS 2224–01	5/6	15/21	26.01	5/7	99.88	0.083	0.057
2MASS 1108+68	46/52	394/536	182.80	5/8	99.75	0.016	0.016
2MASS 0135+12	18/22	110/187	30.00	5/6	99.33	0.041	0.035
2MASS 1658+70	10/13	27/38	31.99	9/14	97.31	0.024	0.019
2MASS 1615+35	12/15	43/61	40.92	6/6	82.69	0.073	0.067
2MASS 0015+35	5/9	21/34	230.31	6/6	80.82	0.026	0.024
2MASS 0058–06	3/3	11/12	26.95	5/5	80.23	0.034	0.028
2MASS 1439+19 <sup>b</sup>	11/11	28/30	38.90	4/4	79.81	0.014	0.013
2MASS 1338+41	27/29	112/140	123.86	8/9	77.10	0.039	0.035
2MASS 1029+16	5/5	14/18	32.96	6/6	30.39	0.057	0.063
2MASS 0036+18	10/18	36/85	53.00	6/8	26.66	0.009	0.010
2MASS 1506+13	3/4	9/12	35.91	5/6	22.46	0.024	0.030
2MASS 1412+16	8/11	27/39	84.92	4/4	11.40	0.018	0.025
2MASS 1146+22AB <sup>a</sup>	10/16	28/48	36.90	5/5	0.54	0.034	0.057
2MASS 1411+39	24/30	78/132	131.86	4/5	0.12	0.047	0.056

<sup>a</sup>Bailer-Jones & Mundt (2001a) detected variations in these objects in their study.

<sup>b</sup>Bailer-Jones & Mundt (2001a) did not detect variations in this object in their study.

Table 3. CLEAN Results for Variable and Possibly Variable Targets

Object	Primary Peak Period [hours]	PNR <sup>a</sup>
2MASS 0746+20AB	31.0±0.1	4.85
2MASS 1300+19	238.±9.	3.38
2MASS 1108+68	23.8±0.1	2.55
2MASS 1658+70	1.89±0.01	1.64
2MASS 0135+12	18.6±0.2	1.48
2MASS 2224−01	21.8±0.4	0.71
2MASS 1439+19	2.60±0.01	1.85
2MASS 1615+35	1.01±0.01	1.24
2MASS 1338+41	6.68±0.01	1.06
2MASS 0015+35	9.12±0.01	0.85
2MASS 0058−06	2.34±0.10	0.74

<sup>a</sup>PNR = ratio of CLEAN peak power to the noise.

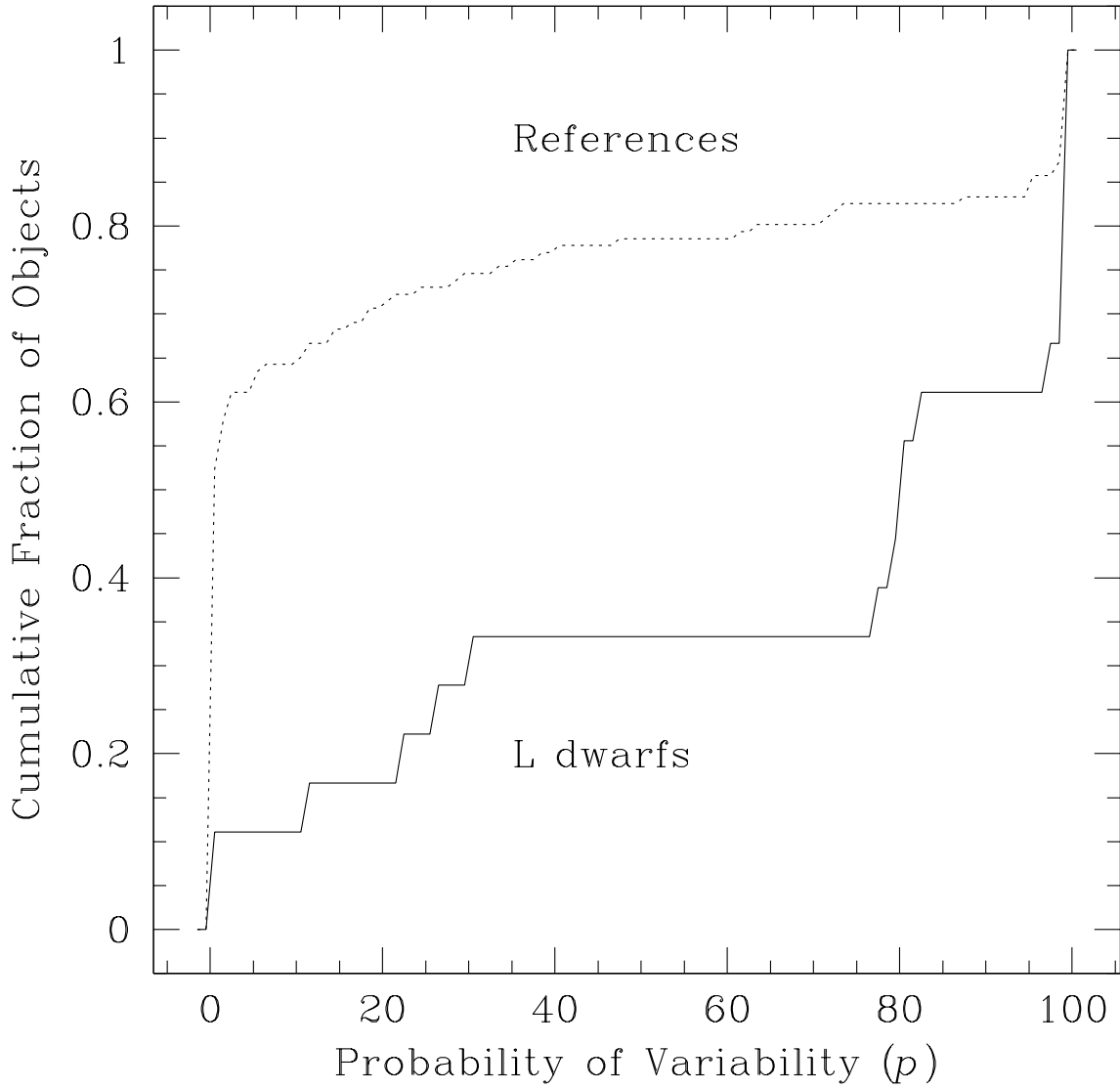


Fig. 1.— Cumulative fraction of L dwarfs (solid line) and reference stars (dotted line) as a function of probability of variability. The clear trend is that the L dwarfs tend to have higher values of  $p$  than the references, indicating that the L dwarfs are more variable.

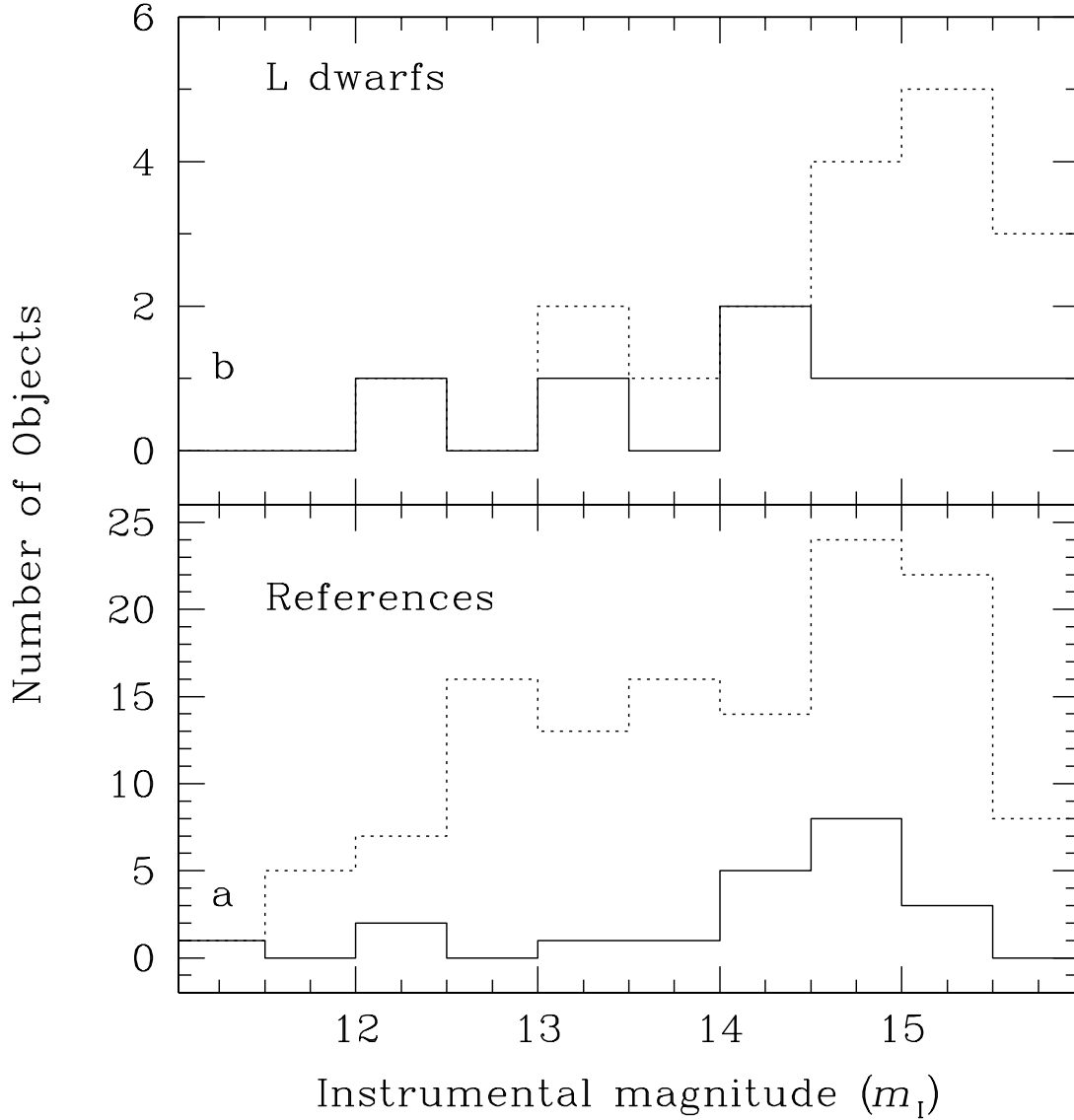


Fig. 2.— a: Histograms of the numbers of variable (solid line) and total (dotted line) references as a function of magnitude. The lack of any systematic trend indicates that we are adequately estimating the photometric errors in these objects. b: Same as panel a except for the L dwarfs.

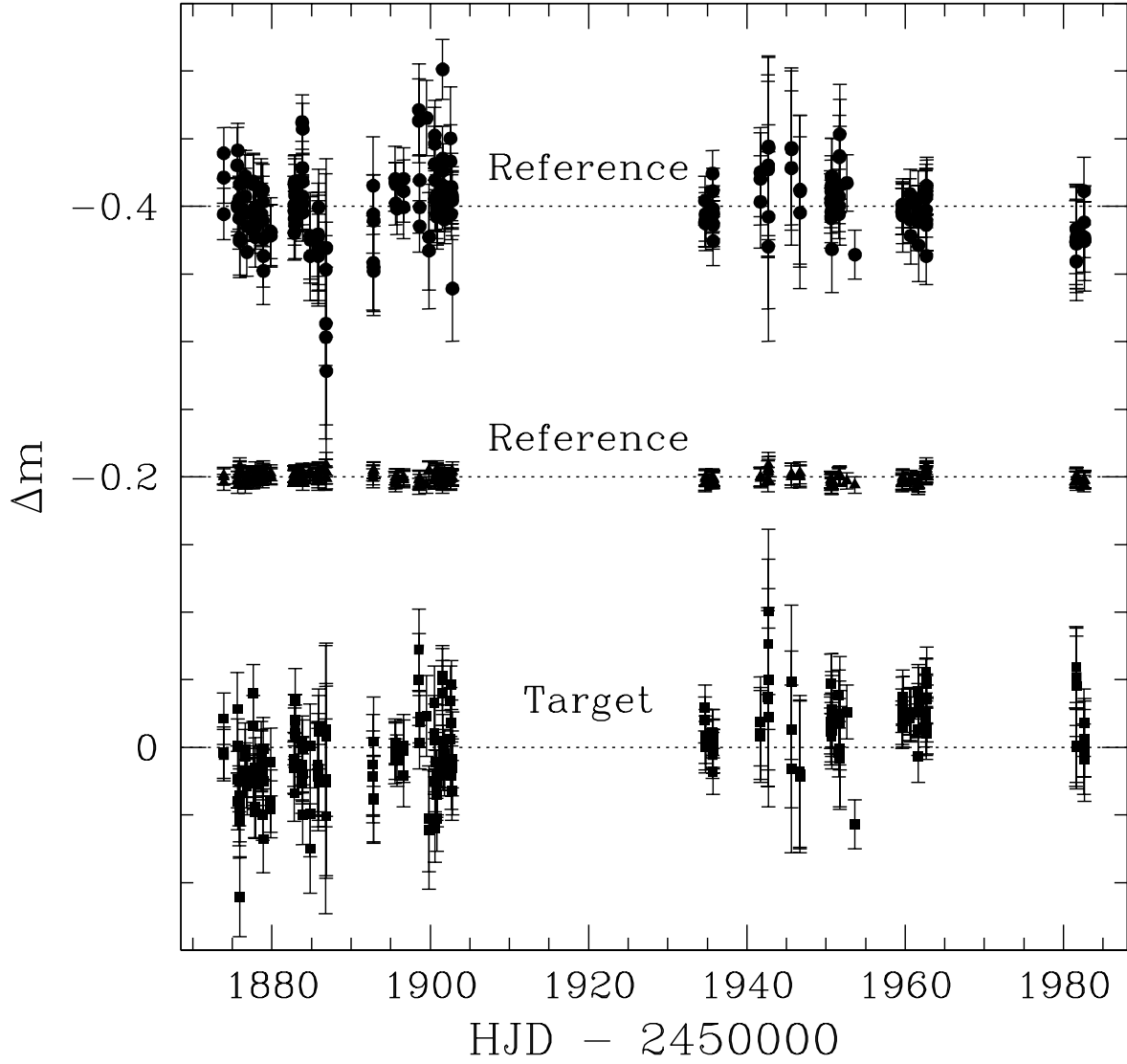


Fig. 3.— Differential magnitude vs. HJD for 2MASS 0345+25 (squares), a bright reference (triangles offset by  $-0.2$  mag) and a faint reference (circles offset by  $-0.4$  mag). Note that up (i.e. more negative  $\Delta m$ ) represents an increase in object brightness.

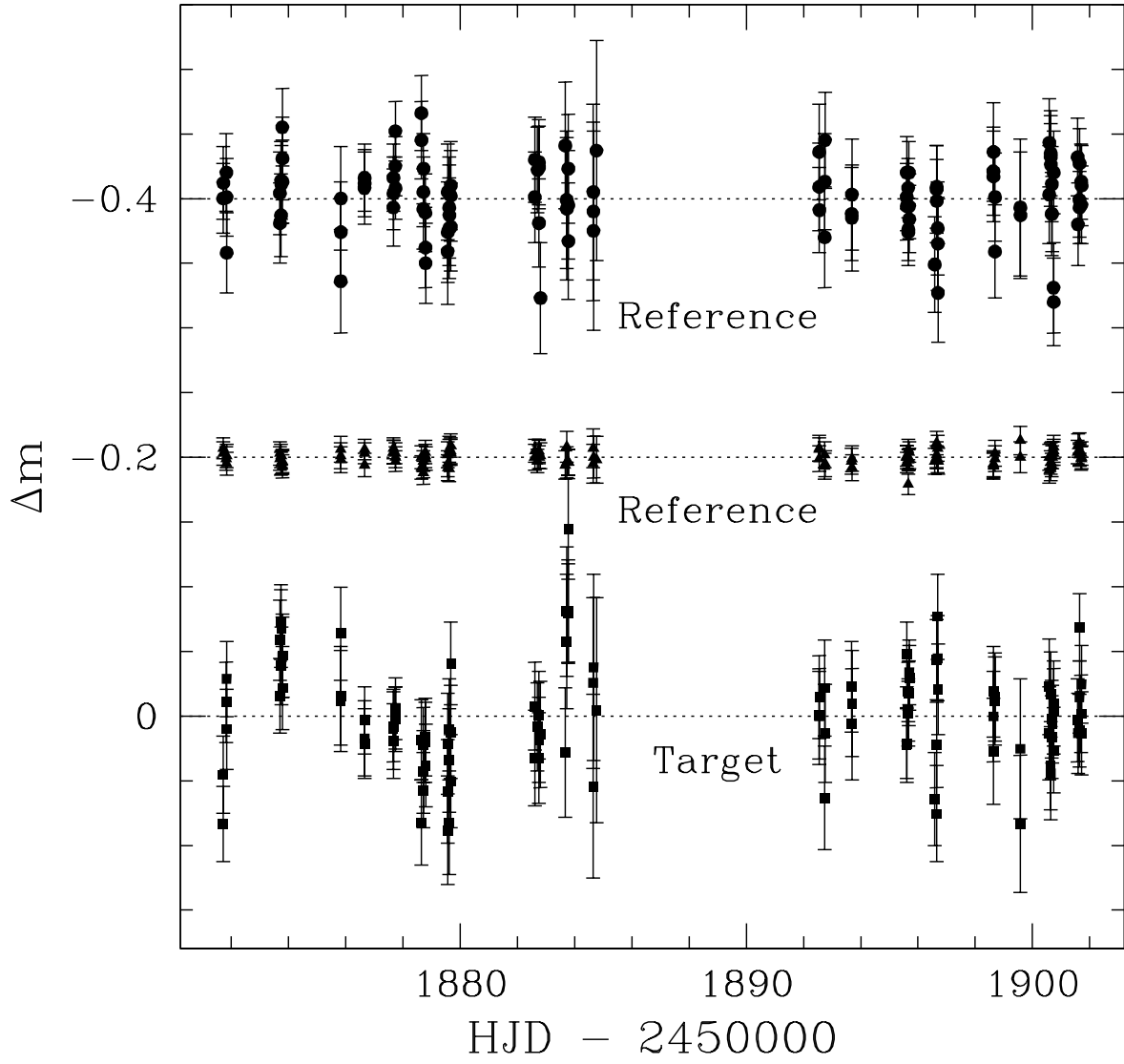


Fig. 4.— Same as Figure 3 except for 2MASS 0135+12.



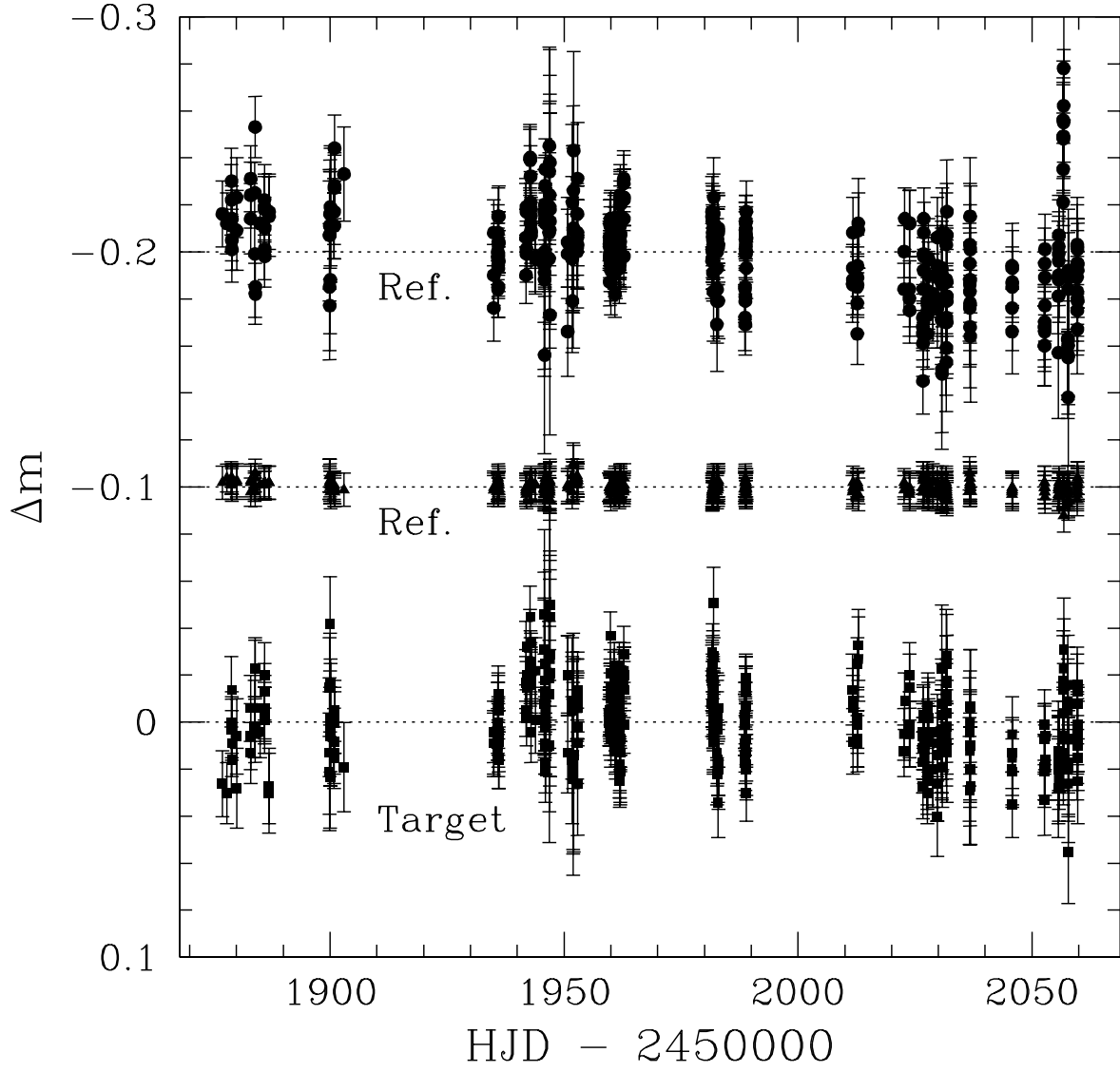


Fig. 5.— Same as Figure 3 except for 2MASS 1108+68 and the bright and faint references are offset by  $-0.1$  and  $-0.2$  mag, respectively.

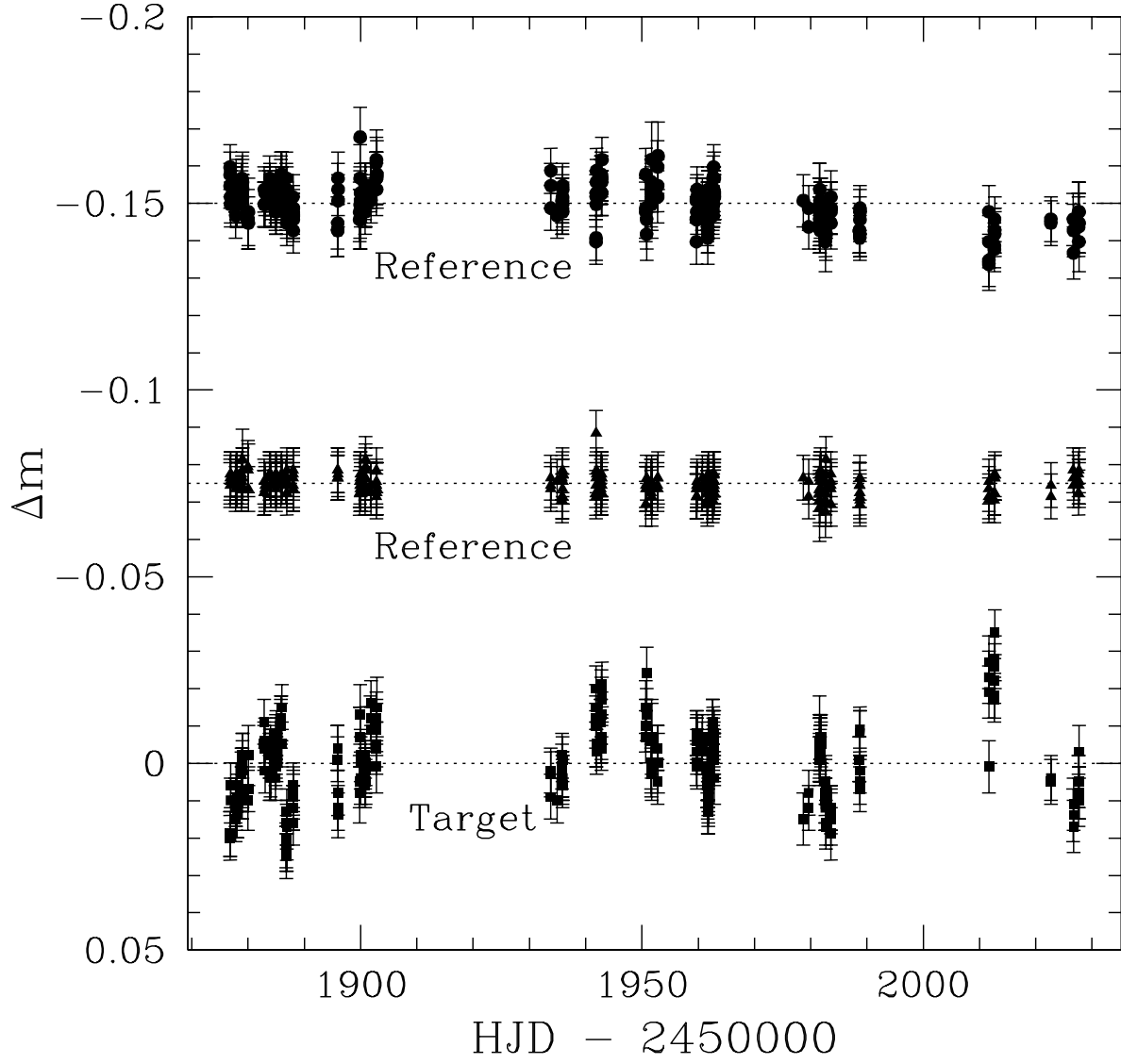


Fig. 6.— Same as Figure 3 except for 2MASS 0746+20AB and the bright and faint references are offset by  $-0.075$  and  $-0.15$  mag, respectively.

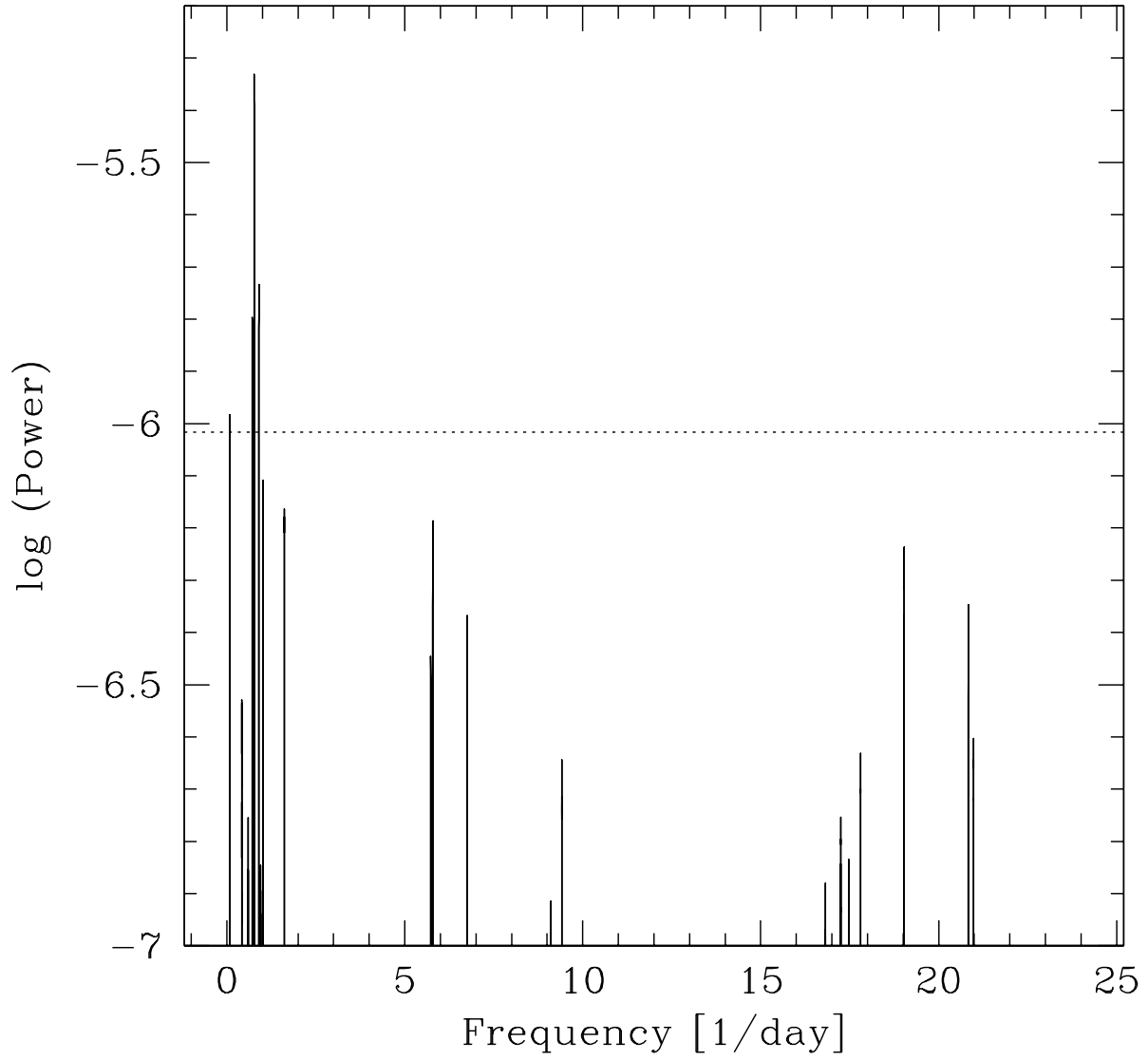


Fig. 7.— Power spectrum of 2MASS 0746+20AB. The dotted line denotes the noise level as defined by the average power of the 1000 random light curves. The peak is located at  $31.0 \pm 0.1$  hours.

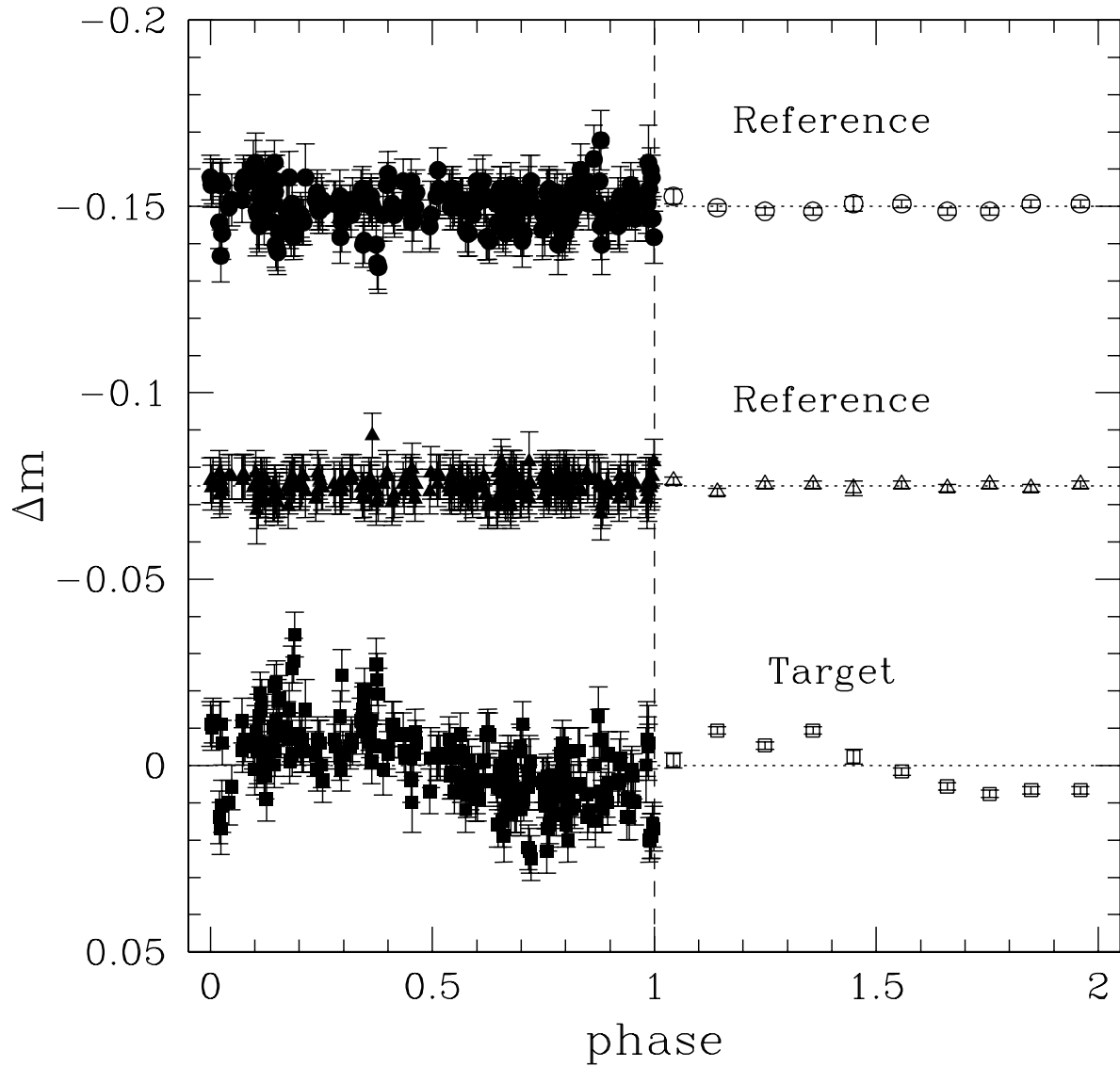


Fig. 8.— Differential magnitude vs. phase for 2MASS 0746+20AB. The points and offsets are the same as in Figure 6 for phase = 0-1; the open symbols from phase = 1-2 are averages of the data from bins 0.1 phase units wide.

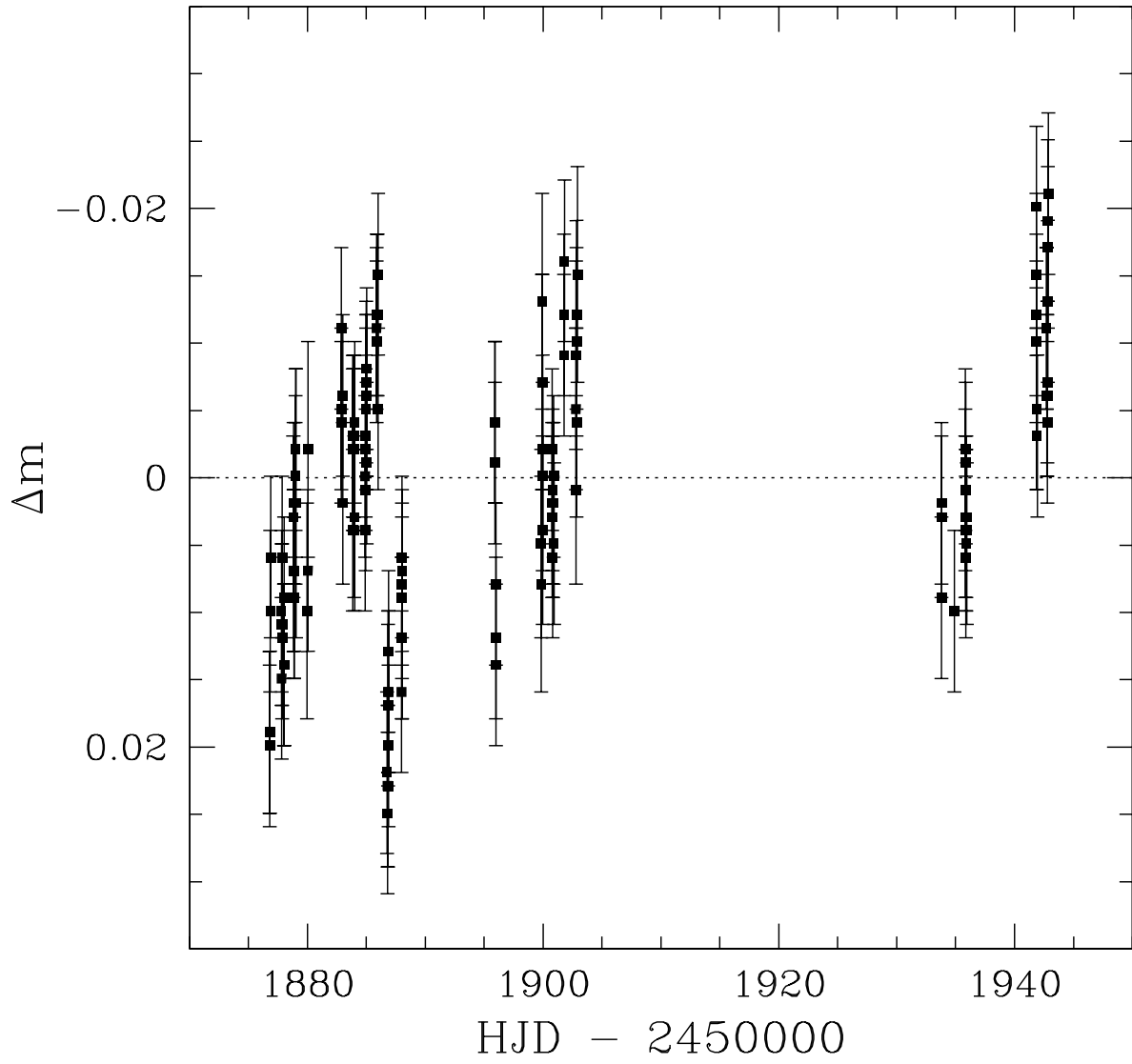


Fig. 9.— Close-up view of the first 70 days in the light curve for 2MASS 0746+20AB.

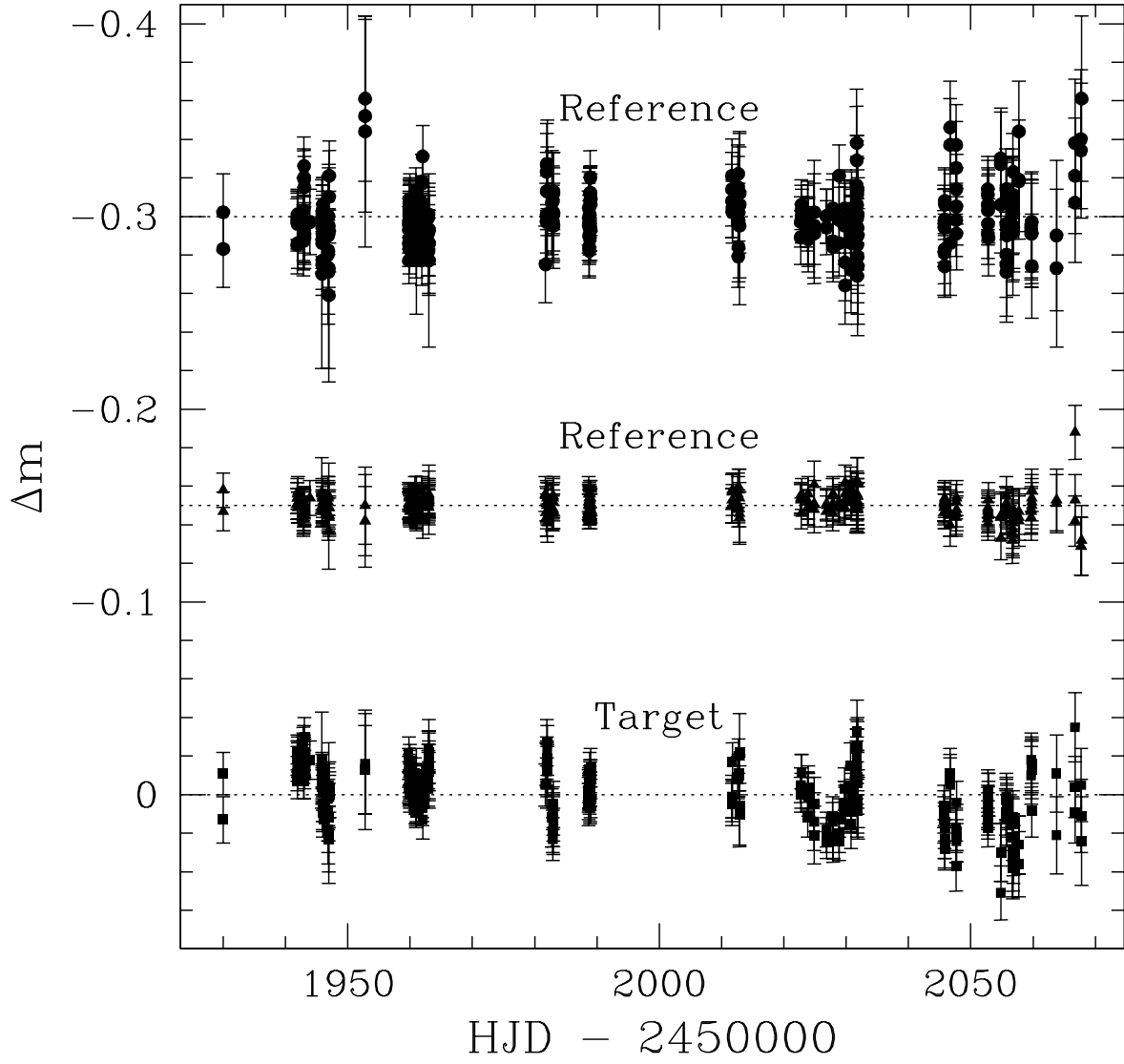


Fig. 10.— Same as Figure 3 except for 2MASS 1300+19 and the bright and faint references are offset by  $-0.15$  and  $-0.3$  mag, respectively.

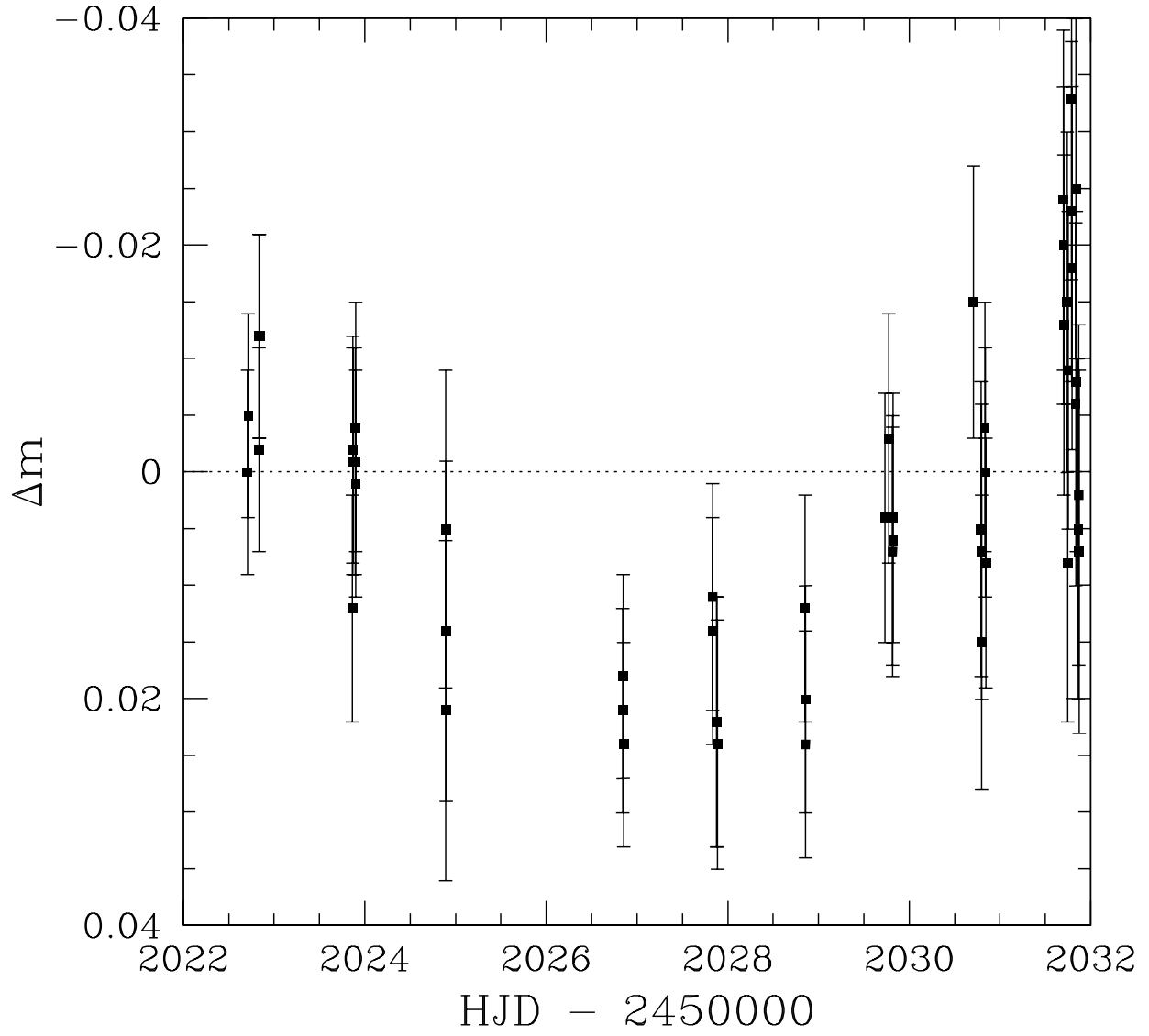


Fig. 11.— Close-up view of the light curve around HJD=2027 for 2MASS 1300+19.

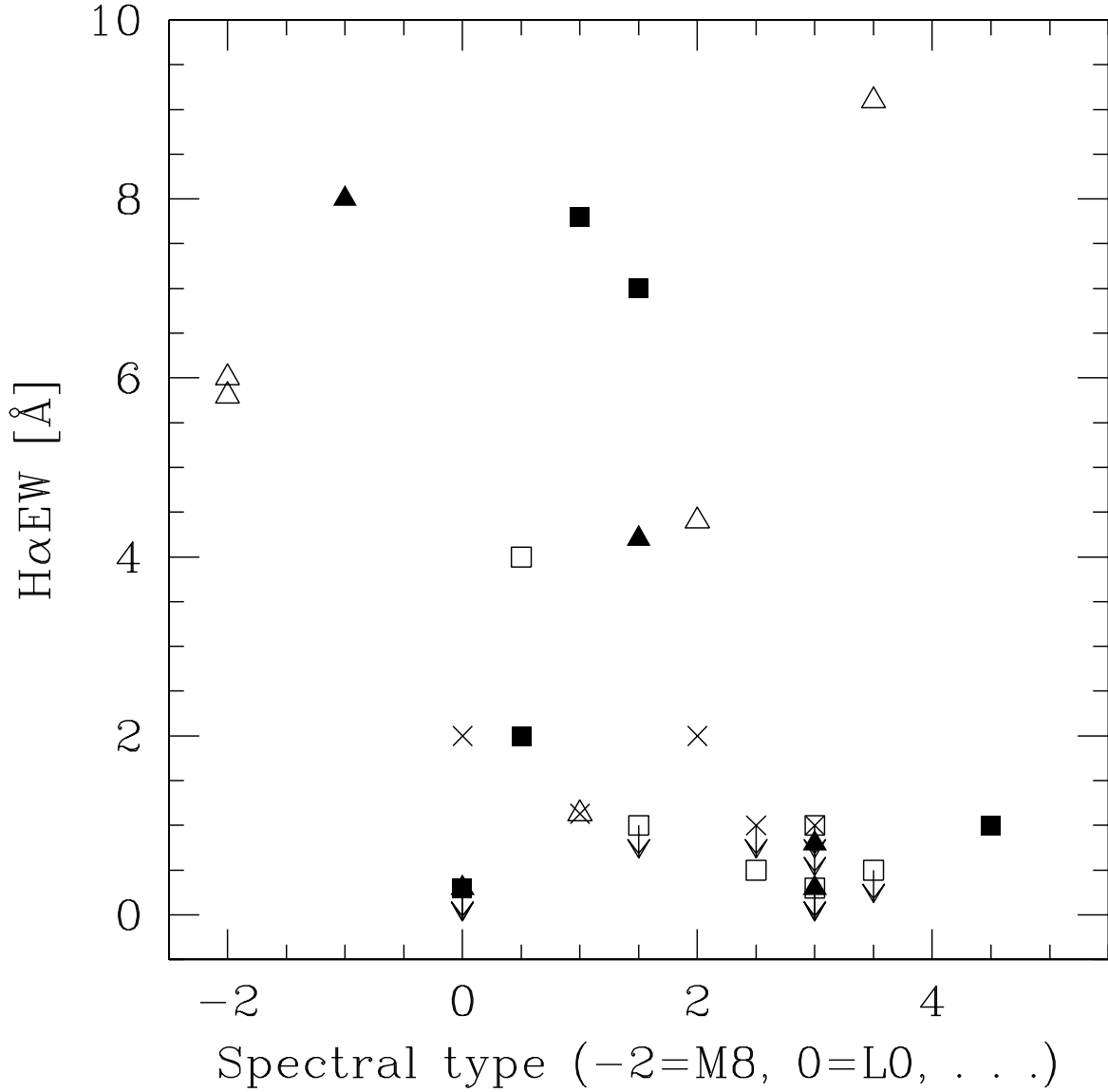


Fig. 12.— H $\alpha$  equivalent width as a function of spectral type for variables (solid symbols), non-variables (open symbols), and possible variables (crosses) from this study (squares) and (Bailer-Jones & Mundt 2001a) (triangles). H $\alpha$  upper limits are shown with arrows. The lack of any trends between variability and H $\alpha$  emission suggests that magnetic activity is not responsible for photometric variability.



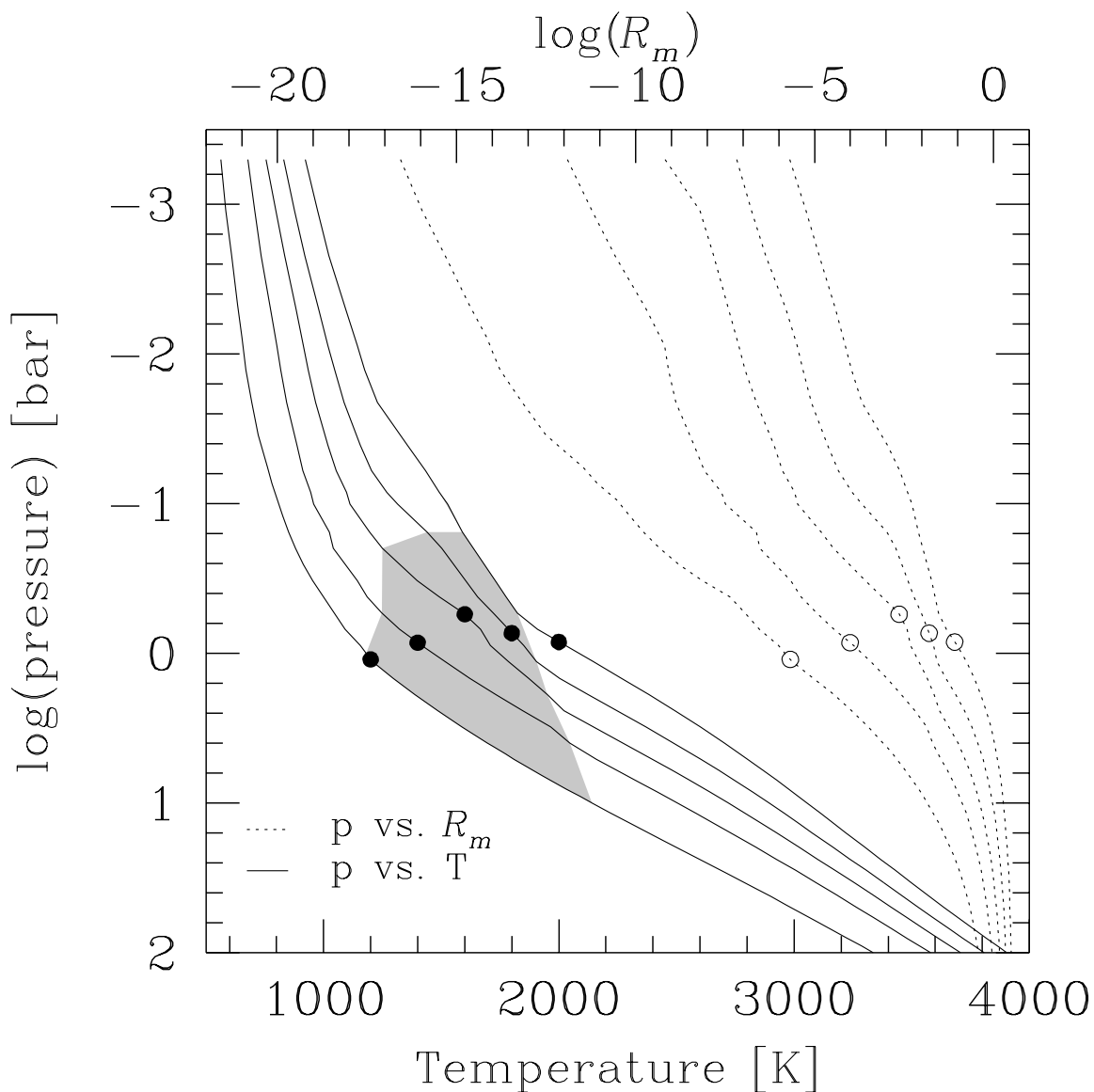


Fig. 13.— Magnetic Reynolds number ( $R_m$ , dotted lines) and temperature (solid lines) plotted as a function of pressure in the atmospheres of L-dwarf models with  $f_{\text{rain}} = 3$  and  $T_{\text{eff}} = 1200, 1400, 1600, 1800, \& 2000$  K (spectral types T1 to L2; Stephens et al. 2001), going from left to right. The solid dots represent the pressure at which the temperature matches  $T_{\text{eff}}$  (approximately the photosphere); open circles are the photosphere location in  $p$  vs.  $R_m$  space; the shaded area is the region from the cloud bottom to cloud top (defined here as the level where the cloud’s integrated optical depth is  $\sim 0.1$ ).  $R_m$  is quite small throughout the entire atmosphere and starts approaching 1 below the base of the clouds and the level of the photosphere.

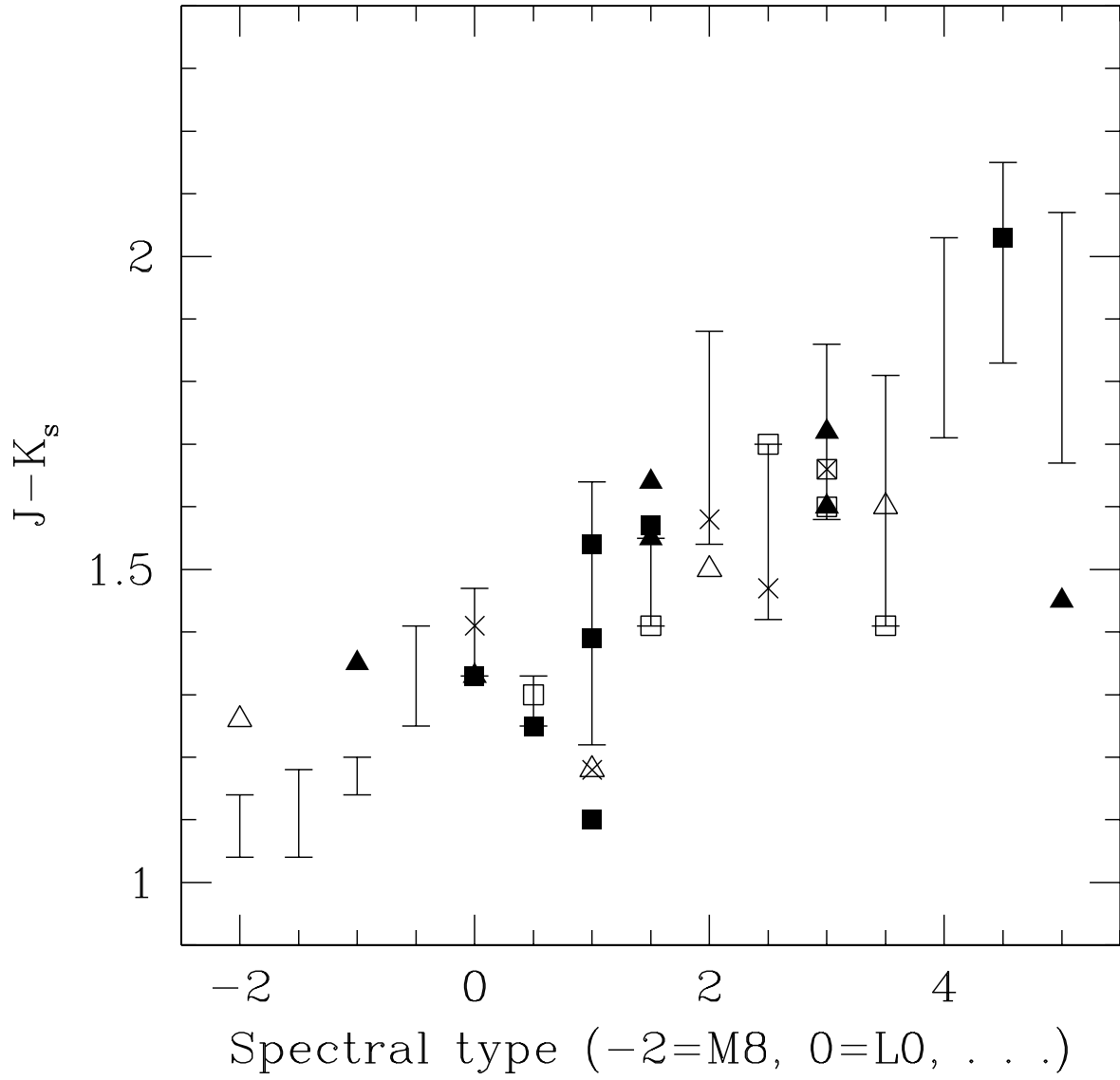


Fig. 14.— 2MASS  $J - K_s$  color as a function of spectral type. The symbols are the same as in Figure 12. No clear trends are seen that distinguish the variable objects from the non-variable objects.